A two-pool mechanism of vesicle release in medial habenula terminals underlies $GABA_B$ receptor-mediated potentiation

Peter Koppensteiner[1*], Pradeep Bhandari[1*], Cihan Önal[1*], Carolina Borges-Merjane[1,2], Elodie Le Monnier[1], Yukihiro Nakamura[3], Tetsushi Sadakata[4], Makoto Sanbo[5], Masumi Hirabayashi[5], Nils Brose[6], Peter Jonas[1], Ryuichi Shigemoto[1]

Author affiliations: [1]Institute of Science and Technology Austria (ISTA), 3400 Klosterneuburg, Austria; [2]Present address: Biozentrum of the University of Basel, 4056 Basel, Switzerland; [3]Department of Pharmacology, Jikei University School of Medicine, Nishishinbashi, Minato-ku, Tokyo, 105-8461, Japan; [4]Advanced Scientific Research Leaders Development Unit, Gunma University Graduate School of Medicine, Maebashi, Gunma 371-8511, Japan; [5]Section of Mammalian Transgenesis, National Institute for Physiological Sciences, Okazaki, 444-8585 Japan. [6]Department of Molecular Neurobiology, Max Planck Institute of Experimental Medicine, 37075 Göttingen, Germany

*These authors contributed equally

Corresponding authors: Ryuichi Shigemoto, e-mail: ryuichi.shigemoto@ist.ac.at

Peter Koppensteiner, e-mail: peter.koppensteiner@ist.ac.at

Abstract

$GABA_B$ receptor (GBR) activation inhibits neurotransmitter release in axon terminals in the brain, except in medial habenula (MHb) terminals, which show robust potentiation. However, mechanisms underlying this enigmatic potentiation remain elusive. Here, we report that GBR activation induces a transition from tonic to phasic release accompanied by a 4-fold increase in readily releasable pool (RRP) size in MHb terminals, mirrored by a similar increase in the docked vesicle number at the presynaptic active zone (AZ). The tonic and phasic release vesicles have distinct coupling distances. We identified two vesicle-associated molecules, synaptoporin and CAPS2, selectively involved in tonic and phasic release, respectively. Synaptoporin mediates augmentation of tonic release and CAPS2 stabilizes readily releasable vesicles during phasic release. A newly developed “Flash and Freeze-fracture” method revealed selective recruitment of CAPS2 to the AZ during phasic release. Thus, we propose a novel two-pool mechanism underlying the GBR-mediated potentiation of release from MHb terminals.

Introduction

The synaptic connection from the medial habenula (MHb) to the interpeduncular nucleus (IPN) is a phylogenetically conserved pathway involved in emotion- and addiction-related behaviors[1-4]. The most striking peculiarity in this pathway is an enhancement of unparalleled scale of neurotransmitter release from terminals originating from cholinergic neurons in the ventral MHb by activation of presynaptic $GABA_B$ receptors (GBRs)[4], usually inhibitory G-protein coupled receptors[5]. Except for an increase in presynaptic Ca^{2+} influx, it is currently unknown which mechanisms mediate this increase in release. Another unique feature of the MHb-IPN synapse is the exclusive use of Cav2.3 for release[1]. However, Cav2.3-mediated release is not necessarily potentiated by GBR activation since it is inhibited in terminals originating in the dorsal MHb[1,6].

Across the nervous system, synaptic terminals respond in either one of two fundamental ways to the repeated excitation at high frequency, facilitation of neurotransmitter release called tonic release, or depression of neurotransmitter release called phasic release[7-9]. While the depression of phasic release is mediated by a depletion of the readily releasable pool (RRP) of synaptic vesicles (SVs), the facilitation of tonic release is likely mediated by a progressive increase in release probability (P_r) by residual Ca^{2+} [7,10]. Although the molecular properties determining the release modes in which a certain synapse type operates are incompletely understood, relevant factors include Ca^{2+} influx, stimulation frequency and the priming and docking states of SVs[7-9,11].

Here, we report that, following GBR activation, MHb terminals transition from a facilitating, tonic to a depressing, phasic neurotransmitter release mode at a physiological stimulation frequency. This transition is induced by a GBR-mediated increase in Ca^{2+} influx, which recruits additional SVs to the RRP. Using “Flash and Freeze” in acute IPN slices, we observed an increase in docked SVs following GBR activation to the same extent as the increase in RRP size. We screened SV-associated proteins expressed in MHb neurons and found synaptoporin and CAPS2 selectively involved in tonic and phasic release, augmenting

release and retaining readily releasable SVs, respectively. Using a new method for nanoscale visualization of membrane-associated proteins within milliseconds after exocytosis, named "Flash and Freeze-fracture", we discovered CAPS2 recruitment to the presynaptic active zone (AZ) and its stabilization there during phasic release.

Results

Transition from tonic to phasic neurotransmitter release by GBR activation

Rodent MHb neurons are active at ~10 Hz *in vivo*[12-14] but postsynaptic responses in IPN neurons following repetitive stimulation of MHb axons at this physiological frequency have never been studied. Therefore, we recorded rostral/central IPN neurons in whole-cell mode and measured excitatory postsynaptic currents (EPSCs) evoked by electrical stimulation of the fasciculus retroflexus (FR), a fiber bundle arising in the habenula. In order to keep the MHb-IPN pathway intact, we prepared 1 mm-thick angled slices as described previously[1] (Fig. 1A). Under baseline conditions, 10–Hz stimulation for three seconds produced EPSC responses that increased in amplitude with consecutive stimuli (Fig. 1B). Application of the GBR agonist R(+)-baclofen (1 µM) greatly potentiated initial EPSC amplitudes in the 10–Hz train but continued stimulation progressively reduced subsequent EPSC amplitudes (Fig. 1B-D). Normalization of EPSC amplitudes to the corresponding first baseline EPSC revealed that the enhanced EPSC amplitudes by baclofen decayed to the level of the facilitated baseline EPSC amplitudes (Fig. 1D). This implies that GBR-mediated depressing neurotransmission occurred in addition to and not instead of the baseline facilitating release. Thus, MHb terminals exhibited a facilitating, tonic neurotransmitter release pattern under baseline conditions and transitioned to a depressing, phasic release pattern after GBR activation.

Ventral MHb terminals co-release glutamate and acetylcholine[15], therefore, we tested whether the tonic and phasic release are selectively mediated by one of the two transmitters. Cholinergic EPSC trains in the presence of the AMPA receptor blocker DNQX (10 µM) still

transitioned to a phasic response pattern after GBR activation (Extended Data Fig. 1A) similar to that of glutamatergic EPSC trains in the presence of cholinergic blockers (50 µM hexamethonium, 5 µM mecamylamine) (Extended Data Fig. 1B). Although the cholinergic RRP size (0.72 ± 0.18 nA, n=8) was much smaller than the glutamatergic one (3.57 ± 0.47 nA, n=8; Extended Data Fig. 1C), cholinergic P_r was not significantly different from that of glutamatergic neurotransmission (Extended Data Fig. 1C). Thus, the GBR-mediated phasic release induction equally affects cholinergic and glutamatergic release, though glutamate mainly contributes to the EPSCs.

We then quantified the recovery from activity-dependent modulations of tonic and phasic release (Fig. 1E, F). The facilitated baseline responses decayed exponentially with a tau of 9.1 s (Fig. 1G), suggesting that this facilitation is augmentation[16]. Similarly, depression of phasic release recovered with a tau of 4.4 s, suggesting that the EPSC decrease results from RRP depletion. In conclusion, the two modes of neurotransmitter release from MHb terminals exhibit distinct short-term plasticity and recover from the activity-dependent modulation within seconds.

Role of presynaptic Ca^{2+} in the GBR-mediated enhancement of neurotransmitter release

We next explored the role of presynaptic Ca^{2+} in the GBR-mediated transition from tonic to phasic release. Using AAV injections into the MHb of ChAT-IRES-Cre mice, we expressed axon-GCaMP6s in cholinergic neurons. FR stimulation at 10 Hz for three seconds increased presynaptic GCaMP fluorescence in the IPN 4.0 ± 0.6 fold of resting fluorescence intensity whereas application of baclofen further increased it 6.5 ± 0.9 fold (n=5 slices, 5 mice; Fig. 2A, B). However, presynaptic GBRs are known to inhibit the influx of Ca^{2+} through voltage-gated Ca^{2+} channels (VGCCs) and no report shows direct GBR-mediated increases in Ca^{2+} influx for any VGCCs in reconstituted systems[5]. Using simulations based on our Ca^{2+} imaging data, we asked whether the increase in presynaptic Ca^{2+} could stem from the inhibition of the Ca^{2+}-binding ability of a buffer, resulting in an “un-buffering” of presynaptic Ca^{2+}, rather than enhanced Ca^{2+} influx (Extended Data Fig. 2, Extended Data Table 1). Analysis of response

kinetics of our experimental GCaMP data revealed significantly faster rise times after baclofen application with no change in decay times (Extended Data Fig. 2A–D). Using GCaMP6s as a model buffer, we simulated Ca^{2+} response kinetics at distinct buffer concentrations and found that high concentrations of a high-affinity Ca^{2+} buffer resulted in significantly prolonged decay times and lower peak fluorescence (Extended Data Fig. 2E–H), ruling out Ca^{2+} un-buffering as the GBR-mediated mechanism. Furthermore, alterations in Ca^{2+} extrusion also failed to reproduce the observed changes in GCaMP fluorescence after baclofen (Extended Data Fig. 2I, J). Finally, we simulated alterations in Ca^{2+} influx and found that a 2.3-fold increase in Ca^{2+} influx most closely reproduced our observed increase in GCaMP peak fluorescence after baclofen (Extended Data Fig. 2K–M).

Since our simulation confirmed increased Ca^{2+} influx as the cause of the GBR-mediated increase in presynaptic GCaMP fluorescence, we next tested whether increasing Ca^{2+} influx by other means was sufficient to induce phasic release. Surprisingly, elevation of extracellular Ca^{2+} from 2.5 to 5 mM or addition of the voltage-gated K^+ channel blockers tetraethylammonium chloride (TEA-Cl, 1 mM) and 4-aminopyridine (4-AP, 100 µM) neither induced phasic release nor occluded its induction by baclofen (Fig. 2C–H). Although TEA/4-AP application strongly enhanced spontaneous neurotransmitter release, evoked EPSC responses remained tonic and exhibited augmentation (Fig. 2F–H). Thus, we conclude that increasing Ca^{2+} influx alone is insufficient to induce phasic release.

We next hypothesized that increased Ca^{2+} influx during phasic release might result in diffusion of Ca^{2+} further away from the Ca^{2+} channel to recruit SVs more distant from the AZ compared to those for baseline tonic release. Therefore, we tested the effect of a slow Ca^{2+} buffer, EGTA-AM (100 µM), on phasic release, first applied after baclofen (Fig. 2I). EGTA-AM selectively reduced the EPSC amplitudes of early responses in the 10–Hz train but the phasic release pattern remained similar (Fig 2J). Specifically, EGTA-AM reduced the first EPSC ($EPSC_1$) amplitude on average by 51.8 ± 2.1% (n=8, 4 mice), suggesting that the phasic release is loosely coupled to Cav2.3[17]. In contrast, EGTA-AM had no significant effect on

baseline $EPSC_1$ amplitudes (Fig. 2L-N), suggesting tight coupling for SVs participating in tonic release. Most strikingly, however, EGTA-AM completely blocked the potentiation of $EPSC_1$ amplitudes when applied before baclofen (Fig. 2L-N), suggesting that the induction of phasic release strongly depends on Ca^{2+} distant from Cav2.3. Although the exact presynaptic concentration of EGTA is unknown in EGTA-AM experiments, it is unlikely that presynaptic EGTA concentrations differed between tonic and phasic release since no modulation of endogenous esterase activity by GBRs has been known. Therefore, these results support our hypothesis that diffusion of Ca^{2+} away from Ca^{2+} channels recruits loosely-coupled SVs to the RRP of phasic release.

In summary, our results suggest that 1) activation of GBRs on MHb terminals induces an increase in Ca^{2+} influx; 2) this Ca^{2+} increase is necessary for the recruitment of phasic SVs from distal sites of the terminal inducing phasic release; 3) however, increasing Ca^{2+} influx alone is not sufficient to induce phasic release; 4) the tonic SVs are more tightly coupled to Cav2.3 than phasic SVs, indicating distinct release sites for these SVs.

Comparison of release properties of tonic and phasic neurotransmission

To determine whether GBR-mediated enhancement of release is ascribable to an increase in P_r, RRP or both, we next compared release properties of basal and GBR-enhanced release by applying 30 stimulations at 100 Hz (Fig. 3A, B). Experiments were performed in the presence of 1 mM kynurenic acid (KA) to avoid AMPA receptor desensitization. The 100–Hz stimulation resulted in the depletion of baseline responses, allowing for the measurement of the tonic RRP in cumulative EPSC amplitude plots[18]. Strikingly, the application of baclofen increased the RRP on average 4.1-fold (Fig. 3C; baseline RRP: 0.58 ± 0.09 nA; baclofen RRP: 2.37 ± 0.36 nA; n=16 recordings/4 mice). In addition, baclofen also increased P_r on average 2.0-fold (Fig. 3D; baseline: 0.086 ± 0.017; baclofen: 0.169 ± 0.024). Altogether, our functional data suggest that tonic and phasic release modes are mediated by two distinct SV pools with different RRP size and coupling tightness, potentially operating in parallel.

Structural correlates of enhanced neurotransmitter release

Our functional data indicated that phasic release is associated with a 4-fold increase in RRP size compared to basal tonic release (Fig. 3). The RRP is an electrophysiological property considered to be structurally reflected by docked SVs in the AZ[19,20]. To test this, we next used timed high-pressure freezing after optogenetic stimulation of MHb terminals in acute slices ("Flash and Freeze"[21]). First, we measured optogenetic responses in IPN neurons of ChAT-ChR2-EYFP mice[15] in 200–µm thick coronal slices (Fig. 4A). In ChAT-ChR2-EYFP mice, we found that 90.2% of all asymmetrical synapses expressed channelrhodopsin2 in the rostral/central IPN region (Extended Data Fig. 3A). Under baseline condition, optogenetic stimulation at 10 Hz produced tonic-like EPSC responses that decayed over time after the 10–Hz train (Fig. 4A, B). However, in contrast to electrically-evoked EPSCs, the first baseline EPSC in the optogenetic train was frequently larger than the subsequent responses. This likely resulted from the desensitizing kinetics of channelrhodopsin which, upon activation from resting state, exhibits an initially larger conductance than during steady-state or repetitive activity[22,23]. Importantly, the application of baclofen induced phasic release, which rapidly depleted during the 10–Hz train and recovered within 10 seconds (Fig. 4A, B).

To distinguish tonic and phasic RRPs, we chose to freeze MHb terminals at two time points in the presence of baclofen; 1) 100 ms after the 10–Hz stimulation (Depletion group) at which time point the phasic RRP should be mostly depleted, and 2) 10 s after the 10–Hz stimulation (Recovery group) at which time point the phasic RRP should have fully recovered (Fig. 4C, D). Control samples were prepared in the same way but without light stimulation or baclofen. Following freeze substitution, we extracted the rostral/central IPN region and prepared serial ultrathin sections (40 nm) for EM imaging (Extended Data Fig. 3B–C; Fig. 4E). We measured SV diameters and found no significant difference between groups (Control: 46.0 ± 1.7 nm, n=16 synapses, 3 mice; 2215 SVs measured; Depletion: 43.4 ± 1.7 nm, n=18 synapses, 3 mice, 2204 SVs measured; Recovery: 43.6 ± 0.9 nm, n=18 synapses, 3 mice, 2539 SVs measured; Fig. 4F). In a defined perimeter around the AZ (see Methods), we then

197 measured the distance from each SV's center to the nearest presynaptic membrane in 5–nm
198 bins. SVs in direct contact with the presynaptic membrane or whose center was within 20–nm
199 distance of the inner leaflet of the membrane were considered docked. In control samples, the
200 peak bins of SVs were in close proximity of the AZ (20 – 40 nm from the membrane) without
201 making contact, thus, considered as loosely-docked[8] (5^{th} – 8^{th} bins in Fig. 4G). The depletion
202 group displayed lower absolute numbers of SVs, particularly at the loosely-docked bins. In
203 contrast, terminals in the recovery group showed a strong increase in docked SVs (first four
204 bins in Fig. 4G). Furthermore, the density of docked SVs in the recovery group (2.34 ± 0.27
205 docked SVs / 10^4 nm^2; n=18 terminals, 3 mice) increased 3.5-fold compared to the depletion
206 group (0.67 ± 0.15 docked SVs / 10^4 nm^2; n=18 terminals, 3 mice; Fig. 4H). The difference in
207 docked SV densities between depletion and recovery groups was similar to the difference in
208 RRP size between tonic and phasic release (4.1-fold, Fig. 3C), supporting that two distinct
209 pools of SVs mainly contribute to each release mode.

210 **SV-associated molecules selectively involved in tonic and phasic release**

211 To test the two-pool mechanism hypothesis, we next aimed to identify vesicle-
212 associated proteins selectively involved in tonic and phasic release. We first investigated the
213 role of synaptoporin (SPO) based on its selective expression in ventral MHb neurons (Allen
214 Brain Atlas). SPO is a vesicular membrane protein and a homologue of synaptophysin[24], but
215 its functional importance remains unknown[25]. In contrast to synaptophysin, SPO was found to
216 co-precipitate with Cav2.3 in a brain-wide proteomics study[26], suggesting that it may be
217 relevant for neurotransmission in MHb terminals which exclusively rely on Cav2.3 for release[1].
218 Immunofluorescence revealed that SPO was expressed in axon-like structures in the
219 rostral/central IPN subnuclei (Fig. 5A), and at the EM level, SPO-labeling was confirmed on
220 SVs in the vast majority of MHb terminals (Fig. 5B, Extended Data Fig. 4A). We then generated
221 SPO KO mice (see Method) and confirmed the specificity of immunolabeling (Fig. 5A). To test
222 the functional role of SPO, we performed whole-cell recordings from IPN neurons in SPO KO
223 mice (Fig. 5C–F). At baseline conditions, augmentation of tonic release appeared strongly

224 impaired compared to wild-type (WT) mice (Fig. 5D). In contrast, baclofen-induced phasic
225 release did not appear different from that of WT and P_r of $EPSC_1$ remained unaltered (Fig. 5E,
226 F; measured by linear regression analysis of cumulative EPSC amplitude plots). Although
227 there was a significant effect of genotype on phasic P_r time course ($F_{1, 690} = 7.599$, $P = 0.006$,
228 two-way ANOVA), Bonferroni post hoc test revealed no significant difference at any stimulation
229 time point. These results suggest that SPO is a mediator of tonic release augmentation and
230 thus, could be a molecular marker specific for tonic release SVs.

231 Phasic release requires the cytosolic Ca^{2+}-dependent activator protein for secretion
232 (CAPS) in the hippocampus[8,27]. Although there are two CAPS isoforms, CAPS1 and CAPS2,
233 only CAPS1 is required for fast, phasic neurotransmission in the hippocampus[27], whereas
234 CAPS2 was found to be involved in the release of neuropeptides and neurotrophic factors[28,29].
235 Since MHb neurons exclusively express CAPS2 but not CAPS1[30], we hypothesized that
236 CAPS2 might be involved in GBR-induced phasic release. Immunofluorescence revealed
237 strong CAPS2 expression in all IPN subnuclei (Fig. 5G) and pre-embedding EM showed
238 CAPS2 labeling on SVs in the vast majority of MHb terminals in the rostral/central IPN (Fig.
239 5H, Extended Data Fig. 4B). Double immunofluorescence showed a large overlap of labeling
240 for CAPS2 with that for SPO (Extended Data Fig. 4C). We then performed whole-cell
241 recordings in CAPS2 KO[27] (Fig. 5I–L). Functionally, tonic release appeared intact, with
242 augmentation similar to that of WT (Fig. 5I, J). However, phasic release was strikingly altered
243 in CAPS2 KO mice (Fig. 5K, L). Specifically, P_r of $EPSC_1$ was reduced almost 10-fold
244 compared to WT (WT $EPSC_1$ P_r: 0.19 ± 0.02, n=13, 5 mice; CAPS2 KO $EPSC_1$ P_r: 0.02 ± 0.00,
245 n=14, 3 mice, Fig. 5L). Furthermore, P_r increased over the first four stimuli before starting to
246 reduce gradually. Interestingly, we observed similar phasic responses in WT mice but only at
247 the very first 10–Hz stimulation in the presence of baclofen (Extended Data Fig. 5A, B).
248 Therefore, these results suggest that CAPS2 is recruited Ca^{2+}-dependently during phasic
249 release induction and might serve to stabilize replenished SVs in a docked state. Nonetheless,
250 the facilitation in the first several stimuli followed by depression in CAPS2 KO mice (Fig. 5K,

L) indicates that CAPS2 does not interfere with the Ca^{2+}-dependent recruitment of phasic release SVs. Overall, we identified SPO and CAPS2 as SV-associated proteins selectively involved in tonic and phasic release, respectively.

Activity-dependent induction and retention of phasic release

Our results in CAPS2 KO mice suggest that CAPS2 is required for the retention of newly recruited SVs in the RRP, but previous activity is necessary for the potentiation of initial EPSCs in the train. Therefore, we tested whether achieving the maximal phasic response is activity-dependent or whether baclofen without activity is sufficient to reach peak potentiation. To this aim, we recorded bilateral MHb inputs to single IPN neurons and, after establishing a baseline response, stopped stimulation on one hemisphere while washing in baclofen (silent washin, Fig. 6A, B). Once the 10–Hz stimulation (3 s, every 20 s) on the other hemisphere induced maximal potentiation, the same 10–Hz stimulation of the silent side resumed (Fig. 6B). Strikingly, $EPSC_1$ amplitude in the first 10–Hz stimulation train was only marginally increased whereas the second train exhibited maximal potentiation of $EPSC_1$ amplitude. This result confirmed that the induction of phasic release is activity-dependent.

Next, we asked whether the GBR-mediated potentiation, once induced, might be stored in the absence of GBR activation during periods of synaptic inactivity. To test this, we stimulated MHb inputs bilaterally to induce phasic release on both sides in the presence of baclofen. Once full potentiation was achieved, stimulation on one hemisphere was halted (silent washout) while starting the washout of baclofen (Fig. 6C). Five minutes after the washout onset, potentiation on the continuously stimulated side was fully reverted (stimulated washout). At this time point, we restarted the 10–Hz stimulation of the silent side and saw only marginal potentiation of $EPSC_1$ amplitudes in the first train ($EPSC_1$: 213.2 ± 62.3% of baseline amplitude, n=9, 4 mice; Fig. 6C). However, in the second train, $EPSC_1$ amplitudes increased to 46.8% of the peak potentiation (second train $EPSC_1$: 374.7 ± 82.8% of baseline amplitude; peak potentiation $EPSC_1$: 801.6 ± 120.4% of baseline amplitude). Therefore, we conclude that the GBR-mediated potentiation can be stored for minutes in the absence of GBR activation,

but the retrieval of this stored potentiation also requires activity, consistent with the idea of Ca^{2+}-dependent recruitment of phasic release SVs.

Recruitment of CAPS2 to the presynaptic active zone by phasic but not tonic release

Given the partial storage of GBR-mediated potentiation for at least five minutes (Fig. 6C), we hypothesized that chemical fixation might be sufficiently fast to capture molecular changes underlying the phasic release induction. Therefore, we next investigated the nano-anatomical location of CAPS2 inside MHb terminals during phasic release. We combined optogenetic stimulation of MHb terminals in acute IPN slices from ChAT-ChR2-EYFP mice and immersion chemical fixation followed by pre-embedding immunolabeling ("Flash and Fix"). Control slices remained unstimulated and unexposed to baclofen whereas the "10 Hz" group received three 10–Hz light stimulations (3 s duration, 10 s intervals) without baclofen and the "10 Hz + Baclofen" group received the same stimulation after a 10 – 15 min pre-incubation in 1 µM baclofen. Immediately after the last stimulation, slices were submerged in a fixative (4% PFA, 0.05% glutaraldehyde, 15% picric acid) for 45 min. Pre-embedding immunolabeling for CAPS2 revealed that CAPS2 was specifically recruited to the presynaptic AZ in the 10 Hz + Baclofen group (Fig. 7A, B; Control: 0.3 ± 0.1 particles/AZ, n=58 profiles, 2 mice; 10 Hz: 0.7 ± 0.1 particles/AZ, n=68 profiles, 2 mice; 10 Hz + Baclofen: 2.6 ± 0.3 particles/AZ, n=60 profiles, 2 mice). This result suggests the recruitment and subsequent stabilization of CAPS2 in the presynaptic AZ during the phasic, but not tonic, release.

"Flash and Freeze-fracture" reveals selective recruitment of CAPS2 to the presynaptic membrane during phasic release

SVs containing SPO or bound by CAPS2 may selectively fuse with the AZ membrane during tonic and phasic release, respectively. However, it is unclear whether all SVs contain SPO and CAPS2 or whether tonic and phasic pools are molecularly non-overlapping. To answer this question, we combined "Flash and Freeze" with freeze-fracture replication and subsequent immunolabeling. This method, which we call "Flash and Freeze-fracture", enables

304 the nanoscale detection of multiple proteins simultaneously in the presynaptic membrane
305 within milliseconds of neurotransmitter release (Fig. 8A).

306 If CAPS2 is exclusively expressed on phasic and SPO exclusively on tonic SVs, then
307 the ratio of CAPS2 to SPO molecules in the presynaptic membrane should shift towards
308 CAPS2 during phasic release. In contrast, if all SVs contain CAPS2 and SPO, the ratio of
309 CAPS2 to SPO molecules in the presynaptic membrane should remain unaltered between
310 tonic and phasic release. Thus, we next quantified the ratio of CAPS2 to SPO in the
311 presynaptic membrane following stimulation by a single 8 ms light pulse in the absence or
312 presence of baclofen. Since phasic SV recruitment is activity-dependent (Extended Data Fig.
313 5A and Fig. 6B), two 10–Hz conditioning stimuli (3–s duration, 10–s interval) were given 10 s
314 prior to the single light pulse. Freezing was timed so that the tissue reached 0 °C 8 ms after
315 light onset and light application continued for an additional 15 ms during freezing. To maximize
316 release and stabilize SV- and membrane-associated proteins in the presynaptic membrane
317 after fusion, slices were stimulated and frozen in the presence of 1 mM TEA-Cl, 100 µM 4-AP
318 and 100 µM dynasore. Because CAPS2 is a cytosolic protein, we incubated replicas with
319 attached tissue in 2% PFA for one hour prior to SDS digestion to crosslink CAPS2 to potential
320 interacting transmembrane proteins. In “Flash and Freeze-fracture” replicas of “stimulation +
321 baclofen” group, the ratio of CAPS2 to SPO (4.56 ± 0.87, n=6 replicas, 205 profiles, 6 mice)
322 was significantly higher than in the unstimulated control group (ACSF, 0.31 ± 0.01, n=3
323 replicas, 153 profiles, 3 mice) and “stimulation” group (1.33 ± 0.48, n=4 replicas, 320 profiles,
324 4 mice; Fig. 8B, C). We confirmed the specificity of replica labeling for SPO and CAPS2 in
325 acute-slice replicas of corresponding KO mice (Extended Data Fig. 6A). The difference in the
326 ratio during phasic release derived from increases in the density of CAPS2 in the presynaptic
327 membrane (Extended Data Fig. 6B) as SPO density was similar across all three groups
328 (Extended Data Fig. 6B), potentially due to high spontaneous neurotransmission in the
329 presence of TEA/4AP (Fig. 2F). Comparison of SPO and CAPS2 particle numbers in individual
330 AZs revealed significant positive correlation in the “stimulation + baclofen” group but not the

331 "stimulation" group (Extended Data Fig. 6C), indicating that baclofen induced a correlated
332 evoked vesicular release of SPO- and CAPS2-associated SVs, whereas release of these two
333 populations was independent in the stimulation only condition. Although control samples also
334 showed a significant correlation, this was likely caused by the frequent absence of CAPS2 in
335 many of the control profiles. Finally, to test for association of SPO and CAPS2 in the AZ, we
336 compared the nearest neighbor distances (NNDs) from CAPS2 to SPO particles with those
337 from real CAPS2 to simulated SPO particles (see Methods). Interestingly, NND analysis
338 revealed no significant association of CAPS2 and SPO in the presynaptic membrane of both
339 "stimulation" and "stimulation + baclofen" groups (Extended Data Fig. 6D), suggesting that
340 fusion sites of CAPS2- and SPO-associated vesicles may not overlap.

341

342 **Discussion**

343 We discovered that activation of GBRs induces a transition from tonic to phasic
344 neurotransmitter release mode in MHb terminals, which coincides with robust potentiation and
345 an increase in action potential-driven Ca^{2+} influx as previously reported[3,4]. During basal
346 release, small Ca^{2+} influx triggers release of tonic SVs close to the VGCC without involving
347 the distal phasic pool. Importantly, we found GBR-mediated recruitment of additional SVs from
348 distal presynaptic regions, resulting in increases in RRP size and docked SVs. We identified
349 SPO and CAPS2 as two SV-associated molecules selectively involved in tonic and phasic
350 release, respectively. The recruitment of phasic release SVs is activity-dependent and their
351 retention at the AZ is CAPS2-dependent. Strikingly, a newly developed "Flash and Freeze-
352 fracture" method revealed selective transfer of CAPS2 to the presynaptic membrane during
353 phasic release. Thereby, we propose a novel two-pool mechanism (Fig. 8D) underlying the
354 unusual GBR-mediated potentiation of neurotransmitter release from MHb terminals.

355 To our knowledge, all currently known synapses release exclusively in a tonic or phasic
356 manner at a given frequency[8,9]. The MHb terminal in the IPN is the only example capable of a
357 rapid and reversible transition between tonic and phasic release modes at the same release

358 frequency. The combination of our functional and structural data indicates that the two modes
359 co-exist in the same terminals with two distinct populations of SVs selectively involved in these
360 two modes. First, the Ca^{2+} imaging of MHb terminals (Fig. 2A-B) showed increased Ca^{2+}
361 signals in all responsive axons but detected no new axons appearing after GBR activation,
362 indicating that the same axons are involved in both tonic and phasic release. Second, “Flash
363 & Freeze” revealed an increase in docked SVs in the vast majority of terminals after recovery
364 from phasic release depletion, whereas the docked SV numbers were similarly low in the
365 control and depletion conditions (Fig. 4H), indicating that single population of terminals
366 increase docked SVs in phasic mode and depleted them to the same level as tonic mode.
367 Third, “Flash & Freeze-fracture” showed that the increased CAPS2 labeling in the phasic mode
368 (Stimulation + Baclofen) always co-localized with SPO labeling at the AZ (Fig. 8B-C, Extended
369 Data Fig. 6C), indicating that the same terminals have CAPS2- and SPO-associated SVs.
370 Fourth, SPO- and CAPS2-deficient mice have selective impairments in tonic and phasic
371 release, respectively (Fig. 5), but the vast majority of MHb terminals were labeled for SPO and
372 CAPS2 with a large overlap (Extended Data Fig. 4), indicating that tonic and phasic SVs co-
373 exist in the same terminals. Fifth, tonic and phasic SVs have distinct coupling tightness,
374 indicating different distances from Cav2.3 in the AZ. Sixth, “Flash & Freeze-fracture” showed
375 a constant level of SPO at the AZ in the presence and absence of baclofen (Extended Data
376 Fig. 6B), indicating GBR-independent release of SPO-associated SVs in both tonic and phasic
377 modes, whereas the drastic increase in CAPS2 number (Fig. 7) and CAPS2/SPO ratio (Fig.
378 8B-C) by baclofen indicates selective recruitment of CAPS2-associated SVs in the phasic
379 mode. In addition, the positive correlation between SPO and CAPS2 numbers in each AZ in
380 the presence but not the absence of baclofen (Extended Data Fig. 6C) suggests that evoked
381 co-release of SPO- and CAPS2-associated SVs occurs only in phasic release. No significant
382 co-localization of CAPS2 and SPO in the AZ membrane also supports separated fusion sites
383 for the two SV populations. These results provide strong support for the two-pool mechanism
384 with distinct SV populations, SPO- and CAPS2-associated ones mediating tonic and phasic
385 release, respectively, in the same MHb terminals.

We interpret the convergence of tonic and phasic release to similar EPSC amplitudes (Fig. 1D) as an indicator of their parallel nature. However, this assumes that the phasic pool depletes completely, which is not described in other phasic synapses at low stimulation frequencies. On one hand, lack of complete depletion in other synapses might be caused by the presence of an “invisible” tonic component that is masked by the depressing phasic pool[16]. On the other hand, in addition to a parallel SV pool model, our results could also be interpreted according to a recently proposed two-step sequential docking model which categorizes SVs into different docking categories but draws them from a single, molecularly homogenous pool[8,31,32]. Under baseline conditions, the majority of SVs may be in a loosely docked state (SV_{LS}) with only a small proportion SVs in a tightly docked, fusion-competent configuration (SV_{TS}). With repeated stimulation, SVs may gradually transition Ca^{2+}-dependently from LS to TS to fusion until a steady-state is reached. Accordingly, baclofen may shift the resting ratio of LS/TS pools towards TS, resulting in a higher proportion of tightly docked SVs at rest. Although the starting pool ratios of LS/TS in tonic and phasic release are different, repeated stimulation in the presence of baclofen would still lead to the same steady-state as during tonic release, resulting in apparent conversion of facilitated tonic and depressed phasic EPSC amplitudes. According to the sequential model, the release pattern of the loosely-docked pool closely matches our partial phasic responses to the first repetitive stimulation in WT and those to all repetitive stimulations in CAPS2 KO. This could suggest that 1) SV transition from a loosely to a tightly docked state during phasic release induction and 2) CAPS2 mediates the tight docking required for the full phasic release. Importantly, however, a selective recruitment of CAPS2 to the AZ during phasic but not tonic release is difficult to explain with a molecularly homogenous SV pool from which all SVs are drawn. The distinct coupling distance of tonic and phasic SVs and no significant co-localization of SPO and CAPS2 in the AZ also favor the parallel model.

Unexpectedly, we identified SPO as a mediator of tonic release augmentation. Until now, no clear functional role of SPO has been described[25]. Synaptoporin (also called

synaptophysin 2) is a homologue of synaptophysin with several molecular distinctions, one of which is the direct binding to Cav2.3 R-type Ca^{2+} channels[26]. It is conceivable that the interaction of SPO with Cav2.3 in MHb terminals underlies the tighter coupling of tonic compared to phasic release vesicles. Furthermore, Cav2.3 might serve as an anchor point for tonic vesicles during augmentation and loss of this anchor might result in impaired recruitment of tonic vesicles to the AZ during tonic release.

Similar to SPO, the function of the cytosolic CAPS2 protein in fast neurotransmission has remained elusive. Although the more widely expressed CAPS1 is a known mediator of phasic release in the hippocampus, CAPS2 KO alone did not induce any alterations in fast neurotransmission[27]. Instead, CAPS2 was found to serve as a mediator of neuropeptide and neurotrophic factor release during development in other brain regions[30,33,]. Therefore, we cannot rule out developmental alterations in MHb terminals of CAPS2 KO. The CAPS2 function found in MHb terminals, which exclusively express CAPS2 isoform[30], may be masked in other synapses expressing both CAPS1 and CAPS2. Approximately 40% of CAPS proteins elude in the membrane fraction in whole-brain lysates and synaptosomal preparations[34], suggesting that they are often membrane-bound. Importantly, CAPS2 is also located on SVs in parallel fiber terminals in the cerebellum[33]. Thus, the recruitment of CAPS2 to the AZ we observed during phasic activity could result from the fusion of CAPS2-associated SVs, although we cannot rule out that cytosolic CAPS2 is recruited to the AZ by other mechanisms. Most strikingly, in WT MHb terminals, phasic release induction was activity-dependent, with the first repetitive stimulation showing a partial phasic response (Extended Data Fig. 5A) but inducing a fully potentiated response to the subsequent repetitive stimulation. In contrast, in CAPS2 KO mice, the repetitive stimulation induced the partial phasic response every time as if it were the first stimulation. These results suggest that phasic vesicles are activity-dependently recruited to the AZ and, upon fusion with the membrane, CAPS2 proteins associated with the fused vesicles remain at the fusion site, potentially via the Ca^{2+} binding C2 and the plexstrin homology (PH) domains[35]. The remaining CAPS2 at the AZ might serve

as docking sites for replenished vesicles via their Munc13 homology (MHD) and MUN domains[35], resulting in an increase in the RRP. Contrary to this hypothesis, a previous study in CAPS1/2-deficient hippocampal cultured neurons found that the PH but not the MUN domain was required for CAPS2-mediated RRP recruitment[36]. In the CAPS2 KO, phasic vesicles have to be recruited to the AZ "from scratch" at every stimulus train, which may be interpreted as synaptic short-term memory loss of prior activity and thus, CAPS2 might be viewed as an engram molecule[37].

Our results suggest that the same somatic firing pattern in the MHb *in vivo* may produce two distinct output signals from IPN neurons. Specifically, phasic release likely induces short-duration burst firing in IPN neurons followed by periods of silence, whereas tonic release may produce prolonged, uninterrupted firing. A main IPN projection target is the median raphe nucleus (MRN)[38-40], a serotonergic center that modulates a multitude of forebrain functions[41]. Interestingly, tonic excitation of MRN neurons via the IPN is hypothesized to disrupt hippocampal theta oscillation through MRN-derived serotonergic innervation[42]. In addition, high-frequency firing GABAergic MRN neurons have been shown to be active in either tonic or phasic rhythms[43]. Similarly, the IPN also projects to the lateral habenula neurons[40] which exhibit a tonic excitation and phasic inhibition patterns during motivation-related behaviors[44]. Interestingly, downregulation of CAPS2 in MHb neurons induces depression-like phenotypes in mice[45]. Thus, tonic and phasic IPN output patterns might modulate forebrain serotonergic signaling through control of raphe activity as well as motivational states through lateral habenula projections.

Furthermore, activation of GBRs on MHb terminals might selectively strengthen inputs from low-frequency (1 Hz) firing cells, as terminals of high frequency (10 Hz) firing MHb cells might rapidly revert to basal release strength following RRP depletion. What could be the source of GABA for the transition to phasic release? Since the vast majority of IPN neurons are GABAergic and innervate each other together with MHb-derived cholinergic inputs[46,47], local GABA release from presynaptic or postsynaptic IPN neurons[3] might regulate their MHb-

driven output through the activation of presynaptic GBRs. Although the trigger for retrograde GABA release is unknown, a coincidence detection mechanism may be envisioned where secondary excitatory projections to the IPN[48] raise ambient GABA concentrations high enough to activate GBRs on MHb terminals.

The surprising two-pool mechanism we discovered raises several questions: Which factors retain CAPS2 in the AZ during phasic release? What is the exact reason for the increased influx of Ca^{2+} during GBR activation? What is the GBR-mediated signaling mechanism necessary for the phasic release induction other than the Ca^{2+} increase? Future studies will be necessary to answer these questions. Overall, our study provides new insights into the mechanisms underlying the unusual potentiation of release by GBRs from MHb terminals and opens up a new regime of presynaptic modulation.

Materials and Methods

Animals

Wild-type C57BL6J (#000664), heterozygous ChAT-ChR2-EYFP (#014546) and heterozygous ChAT-IRES-Cre (#006410) mice were purchased from Jackson Laboratory. Homozygous CAPS2 KO mice were generated as previously described[27]. Synaptoporin (MGI:1919253) KO mice were generated using the CRISPR-Cas9 method with AAGTACCGCGAAAACAACCGGGG as a guide RNA target sequence. The single-guide RNA and Cas9 protein were co-injected into fertilized oocytes, collected from superovulated C57BL/6J female mice mated with male mice. All the surviving zygotes were transferred into oviductal ampullae of pseudopregnant recipient mice. To determine the genotype of pups, genomic DNA was extracted from ear tissues, and screened by PCR analysis and subsequent direct sequencing analyses. A homozygous 2-bp deletion at amino acid position 130 resulted in a STOP codon at amino acid position 136, which corresponds to the start of the third transmembrane domain[49]. Male and female mice were used indiscriminately in all

493 experiments. Mice were bred and maintained at the preclinical facility at Institute of Science
494 and Technology Austria on a 12h light/dark cycle with access to food and water *ad libitum*. All
495 experiments were performed in strict accordance with the license approved by the Austrian
496 Federal Ministry of Science and Research (Animal license number: BMWFW-66.018/0012-
497 WF/V/3b/2016) and Austrian and EU animal laws.

498

499 **Electrophysiology**

500 Mice (6 – 12 weeks of age) were deeply anesthetized via intraperitoneal (i.p.) injection
501 of ketamine (90 mg/kg) and xylazine (4.5 mg/kg), followed by transcardial perfusion with ice-
502 cold, oxygenated (95% O2, 5% CO2) artificial cerebrospinal fluid (ACSF) containing (in mM):
503 118 NaCl, 2.5 KCl, 1.25 NaH_2PO_4, 1.5 $MgSO_4$, 1 $CaCl_2$, 10 Glucose, 3 Myo-inositol, 30
504 Sucrose, 30 $NaHCO_3$; pH = 7.4. As described previously [1], the brain was rapidly excised and
505 a single, 52–54° angled slice of 1 mm thickness containing the whole MHb to IPN pathway
506 was cut using a Pro7 Linear Slicer (Dosaka, Kyoto, Japan). Slices were left to recover for 20
507 min at 35°C, followed by a slow cool down to room temperature (RT, 22.5 – 24.0 °C) over 40
508 – 60 min. After recovery, the slice was transferred to the recording chamber and superfused
509 with ACSF containing 2.5 mM $CaCl_2$ and 20 µM bicuculline methiodide (Tocris, Bristol, UK) at
510 a rate of 3 – 4 ml/min at RT. Glass pipettes (B150-86-10, Sutter Instrument, Novato, CA, USA)
511 with resistances of 3 – 4 MΩ were crafted using a P1000 horizontal pipette puller (Sutter
512 Instrument) and filled with internal solution containing (in mM): 130 K-Gluconate, 10 KCl, 2
513 $MgCl_2$, 2 MgATP, 0.2 NaGTP, 0.5 EGTA, 10 HEPES, 5 QX314-Cl; pH 7.4 adjusted with KOH.
514 Neurons of the rostral and central IPN were visually identified using an infrared differential
515 interference contrast video system in a BX51 microscope (Olympus, Tokyo, Japan). Electrical
516 signals were acquired at 20 – 50 kHz and filtered at 4 kHz using a Multiclamp 700B amplifier
517 connected to a Digidata 1440A digitizer (Molecular Devices, San Jose, CA, USA) with
518 pClamp10 software (Molecular Devices). Stimulating electrodes (CBBPC75, FHC, Bowdoin,
519 ME) were placed bilaterally on the fasciculus retroflexus and electrical stimulation (10 Hz, 3

seconds, 0.2 ms pulse duration, 0.5 – 2.5 V stimulation intensity) of left or right habenular axon fiber tracts was applied via a stimulus isolator (AMPI, Jerusalem, Israel). Neurons were voltage-clamped at –60 mV in whole-cell mode. Recordings with access resistances exceeding 20 MΩ or with changes in access resistance or holding current by more than 20% were discarded. Access resistance was not compensated. At each sweep, left and right fiber tracts were stimulated separately with 5–s intervals and inter-sweep intervals of 20 s. Left- and right-side derived EPSC responses were treated as individual recordings, meaning that one whole-cell recording of one IPN neuron receiving two independently stimulated inputs would yield n = 2. Tonic and phasic release traces were analyzed after averaging the responses of 5 – 10 sweeps. EPSC amplitudes were measured as the maximal negative current deflection between two stimulation artifacts (or within 100 ms in case of the last stimulus). For time course measurements of recovery from augmentation and depletion, the left or right fasciculus retroflexus was stimulated in separate recordings at 10 Hz for 3 s followed by a single stimulus at intervals from 0.5 – 13.3 s. To calculate RRP size and P_r using cumulative EPSC amplitudes, a linear correlation was fit through the last six points of the cumulative EPSC amplitude plot (stimulus #25 – stimulus #30) and the projected value of the line at x=1 was considered the RRP size (I_{RRP}). Release probability was calculated as $P_r = \frac{I_{EPSC}}{I_{RRP}}$. At 100–Hz trains, the latency of the first baseline EPSC often exceeded the stimulation interval (10 ms) and, therefore, I_{EPSC1} under baseline and baclofen conditions was obtained from separately recorded 10–Hz trains in the same cell. In EGTA-AM experiments, 10 – 15 ml of ACSF containing 100 µM EGTA-AM were recycled continuously over the course of the application and only one cell per slice was recorded. To record optogenetically-evoked EPSCs, 200–µm thick coronal sections of ChAT-ChR2-EYFP mice were cut and light was applied via a pE-300 LED light source (CoolLED, Andover, UK) through the objective at 10 – 20 mW/cm^2 (5 ms pulse duration).

Stereotaxic surgery, AAV injection and calcium imaging

Adult (8 – 10 week old) ChAT-IRES-Cre mice were deeply anesthetized via i.p. injection of ketamine (90 mg/kg) and xylazine (4.5 mg/kg) followed by head fixation in the stereotaxic setup. Using a nanoliter injector (World Precision Instruments, Sarasota, FL, USA), AAV9-hSynapsin1-FLEx-axon-GCaMP6s (Addgene #112010) was injected bilaterally into the MHb at a rate of 50 nl/min for 10 min to the following coordinates (in mm from Bregma): -1.45 anterior/posterior, 0.6 lateral, -2.65 dorsal/ventral; angled at 20°. Animals were left to recover for 3 – 4 weeks and then, 1 mm thick slices were prepared and recovered as described in the electrophysiology section. After recovery, slices were transferred to the recording chamber and superfused with ACSF containing 2.5 mM Ca^{2+} at RT. Stimulating electrodes were placed bilaterally on the fasciculus retroflexus. Widefield imaging of MHb axons in the rostral/central IPN was done using a 20X 0.5NA water-immersion objective (Olympus) and a monochrome CCD camera (XM10, Olympus). To visualize the axon-GCaMP6s, blue light was emitted from a pE-300 led light source (CoolLED) through a fluorescent cube with excitation filter 460-490 nm, dichroic mirror 505 nm and barrier filter 510 nm (U-MWIB2, Olympus). GCaMP fluorescence in response to 10–Hz electrical stimulation (3–s duration, 0.2–ms pulse width, 0.5 – 2.5 V stimulation intensity) was recorded before and during the application of baclofen (1 μM). Full field-of-view frames were captured at 3 Hz and illumination was turned off in between sweeps (20–s sweep intervals).

Calcium imaging-based modeling

For modeling, a Java-based simulator called D3D[50], running on a Windows 10 operating system was used to calculate Ca^{2+} binding with several Ca^{2+} buffer species including GCaMP6. Assuming imaging from a whole presynaptic terminal, we allocated 16 VGCCs [1] in a single compartment (1 × 0.5 × 0.5 μm). In response to a single action potential (AP), each channel was allowed to carry Ca^{2+} current in a Gaussian shape. The peak amplitude was set to 0.3 pA[51,52]. The half-duration of the current was adjusted to reproduce the amplitude of the

GCaMP6 fluorescent change after 10–Hz trains of 30 consecutive APs under baseline condition. The concentration of Ca^{2+}-bound GCaMP6 was converted to a fluorescence change $\Delta F/F$. We assumed that the two Ca^{2+} binding sites in GCaMP6 protein bind Ca^{2+} independently. All simulation parameters are summarized in Extended Data Table 1.

Timed high-pressure freezing after optogenetic stimulation and freeze substitution ("Flash and Freeze")

ChAT-ChR2-EYFP mice (8 – 10 weeks old) were deeply anesthetized, transcardially perfused and the brain was excised as described above. 200–µm thick coronal sections containing the IPN were cut and the IPN was trimmed using a razor blade. Trimmed IPN sections were left to recover as described above, followed by a 10 – 15 min incubation in ACSF containing 2.5 mM Ca^{2+} and 1 µM baclofen. Thereafter, sections were moved to the same ACSF containing 15% polyvinylpyrrolidone (PVP) followed by immediate assembly into a sapphire glass sandwich, consisting of two sapphire discs separated by a 200–µm thick spacer ring and a 400–µm thick spacer ring on the outside (Wohlwend GmbH, Switzerland), into a CLEM middle plate (Leica, Wetzlar, Germany) as described in Borges-Merjane et al. 2020[21]. After trimming, slices were never touched directly and slice transfers between solutions or into the sapphire sandwich were carried out by careful pipetting using a handcrafted, flame-polished glass pipette. The sandwich was inserted into the ICE high-pressure freezer (Leica EM) and slices were optogenetically stimulated three times at 10 Hz (3–s duration, 5–ms pulse width, 10–s interval, measured light intensity 5.9 – 10 mW/mm^2). Slices were rapidly frozen either 100 ms (depletion group) or 10 s after the third 10–Hz stimulation (recovery group). Control group slices were not incubated in baclofen and remained unstimulated.

Freeze substitution was performed as described previously[21]. In brief, frozen sapphire sandwiches were incubated acetone containing 0.1% tannic acid at –90 °C for 20 – 24 h inside

599 an AFS machine (Leica) under constant agitation. Thereafter, samples were washed with
600 acetone (–90 °C) followed by incubation in acetone containing 2% osmium tetroxide and 0.2%
601 uranyl acetate (AL-Labortechnik, Zeillern, Germany). Under continuing constant agitation,
602 samples were then slowly warmed up to 0 °C in three steps: 1) from –90 °C to –60 °C over 2
603 h, incubation at –60 °C for 3 h; 2) from –60 °C to –30 °C over 4 h, incubation at –30 °C for 3
604 h; 3) from –30 °C to 0 over 3 h. Subsequently, slices were removed from the AFS machine,
605 washed with acetone and propylene oxide and incubated in Durcupan resin (Sigma Aldrich;
606 mixture of components A, B, C and D in proportion of 10:10:0.3:0.3, respectively) overnight
607 (O/N). As slight improvement of the original Flash and Freeze method in acute slices, we
608 performed an additional flat embedding step to precisely extract IPN subnuclei for further
609 processing (Extended Data Fig. 3A). For flat embedding, each slice was placed on a silicon-
610 coated glass slide, covered with an ACLAR® fluoropolymer film (Science Services, Munich,
611 Germany) and incubated at 37 °C (1 h) followed by incubation at 60 °C (2 O/N). Using a razor
612 blade, the rostral/central subnuclei were excised from the flat embedded slice, placed into a
613 plastic tube (TAAB Laboratories Equipment Ltd., Aldermaston, UK) and re-embedded in
614 Durcupan resin followed by incubation at 60 °C for 2 O/N. The resulting block was trimmed
615 using a TRIM2 (Leica EM) and serial ultrathin sections (40 nm) were cut using a UC7
616 ultramicrotome (Leica EM). Finally, sections were post-stained with 2% uranyl acetate for 10
617 min and lead citrate for 2 min.

618

619 **“Flash and Freeze-fracture” and replica immunolabeling**

620 Acutely cut IPN slices from ChAT-ChR2-EYFP mice were prepared, trimmed and
621 recovered as described for “Flash and Freeze”. After recovery, slices were incubated in ACSF
622 containing 1 mM Ca^{2+}, 1 mM TEA-Cl and 100 µM 4-AP with or without 1 µM baclofen for 5 –
623 10 min. Thereafter, slices were moved to the same ACSF containing 2.5 mM Ca^{2+}, 100 µM
624 dynasore (HelloBio, Bristol, UK) and 15% PVP followed by assembly of the freezing sandwich
625 consisting of a custom-made, gold-coated copper carrier, double-sided tape (150–µm

626 thickness) and a sapphire disc. After insertion into the ICE high-pressure freezer (Leica EM),
627 slices were stimulated twice at 10 Hz (5–ms pulse width, 3–s duration, 10–s interval), followed
628 by a single light pulse (8–ms duration) and high-pressure freezing, timed so that the sample
629 reached 0 °C exactly 8–ms after light stimulation onset. Light application continued for another
630 15 ms during the freezing process.

631 For freeze-fracture replication, a single metal-sapphire sandwich was inserted into an
632 ACE900 freeze-fracture machine (Leica EM) and warmed up to –120 °C for 20 min under high
633 vacuum of < 8 x 10^{-7} bar. Thereafter, the frozen tissue was fractured by moving the knife
634 through the double-sided tape between the metal carrier and the sapphire disc. After fracture,
635 carbon/platinum replication was performed as described previously[1]. Briefly, a 5-nm layer of
636 carbon angled at 90° was evaporated onto the fracture slice, followed a 2-nm layer of platinum
637 angled at 60° and a final 20-nm layer of carbon at 90°. After removal of the replica from the
638 machine, slices were transferred to 0.1 M phosphate buffer (PB) containing 2% PFA for post-
639 fixation for 1 h, followed by tissue digestion in a solution containing 2.5 % SDS, 20% sucrose
640 in 15 mM Tris buffer (pH 8.3) at 80 °C for 18 h under gentle agitation (50 rpm).

641 Following the SDS treatment, immunolabeling of replicas was performed as described
642 previously[1]. In brief, replicas were washed in washing buffer containing 0.1% Tween-20,
643 0.05% BSA, 0.05% NaN_3 in tris-buffered saline (TBS), pH 7.4. Thereafter, replicas were
644 incubated in the same solution containing 5% BSA (blocking buffer) for 1 h and then incubated
645 in the same solution containing 1% BSA and primary antibodies: guinea pig anti-CAPS2 (8
646 µg/ml)[33] and rabbit anti-synaptoporin (6 µg/ml; SySy, Göttingen, Germany) for 24 h. Replicas
647 were then washed, blocked and finally incubated in secondary antibody solution (washing
648 buffer + 5% BSA) containing 5–nm gold-conjugated anti-rabbit and 10–nm gold-conjugated
649 anti-guinea pig antibodies (both diluted 1:30, BBI Solutions, Cardiff, UK) for 1 O/N. The next
650 day, replicas were washed, mounted onto EM grids and dried, followed by observation in a
651 Tecnai12 transmission electron microscope (FEI Company, Hilsboro, OR, USA) at an
652 accelerating voltage of 120 kV.

653

654 **Immunohistochemistry**

655 50–µm thick sections (perfused with 4% PFA) were washed in 25 mM phosphate-
656 buffered saline (PBS) and incubated in blocking buffer containing 10% normal goat serum,
657 2% BSA and 0.5% triton-X 100 in 25 mM PBS for one hour, followed by O/N incubation in
658 primary antibodies in the same buffer: anti-CAPS2 (0.5 µg/ml) or anti-synaptoporin (1 µg/ml).
659 Slices were then washed and incubated in blocking buffer containing secondary antibodies
660 [1:500, Alexa-488 anti-guinea pig (Molecular Probes, Eugene, OR) or Alexa-488 anti-rabbit
661 (Molecular probes)]. Washed sections were mounted on glass slides in Mowiol (Sigma Aldrich)
662 and observed with an LSM 800 confocal microscope (Zeiss, Oberkochen, Germany).

663

664 **Pre-embedding immunolabeling for EM**

665 Pre-embedding immunolabeling was performed as described previously[1]. Briefly, 50–
666 µm thick IPN slices (from 4% PFA and 0.05% glutaraldehyde perfused brains) were
667 cryoprotected in a series of 5%, 15% and 20% sucrose in 0.1 M PB. Sections were then rapidly
668 frozen in liquid nitrogen and immediately thawed three times. Freeze-thawed sections were
669 treated with 50 mM glycine (Sigma Aldrich) in 50 mM TBS and were washed in TBS. Then,
670 the sections were blocked in 2% BSA with 10% NGS in TBS followed by incubation in primary
671 antibodies (guinea pig anti-CAPS2 (0.5 µg/ml) or rabbit anti-synaptoporin (1 µg/ml) or rabbit
672 anti-GFP (Abcam, USA) in 2% BSA in TBS at 4 °C for 2 O/N and respective 1.4 nm gold-
673 conjugated secondary antibodies (Nanoprobes Inc., USA) for silver intensification or in
674 biotinylated anti-rabbit secondary antibody (Vector Labs, USA) for horseradish peroxidase
675 (HRP) reaction for 1 ON at 4 °C. After washing in TBS and PBS, sections were post-fixed in
676 1% glutaraldehyde in PBS, washed with 50 mM glycine in PBS followed by another wash in
677 PBS.

Silver intensification: Sections were washed in MQ water and silver intensification was performed using a commercial kit (Nanoprobes Inc., USA). Equal drops of component A (initiator) and component B (moderator) were mixed and vortexed, followed by the addition of component C (activator). After vortexing all three components properly, sections were incubated in this solution in the dark. The silver intensification reaction was stopped by adding MQ water and sections were washed with 0.1 M PB.

HRP reaction: Sections were washed in TBS followed by incubation in avidin-biotin complex (ABC) solution (Vector Laboratories, USA) for two hours. ABC solution was prepared 30 min prior by adding 1% avidin (A) to TBS, followed by addition of 1% biotin (B). After washing with TBS and tris-buffer (TB), sections were incubated in 0.05% di-amino benzidine (DAB) (VWR, Radnor, PA, USA) in TB for 15 min in the dark. Then, H_2O_2 was added to a final concentration of 0.003%. After a dark coloring became visible in the IPN, the hydrogen peroxidase reaction was stopped by adding TB. Finally, sections were washed with 0.1 M PB.

After washing sections in 0.1 M PB after silver intensification or HRP reaction, sections were fixed with 1% osmium tetroxide in 0.1 M PB for 20 min in the dark. Sections were then washed in MQ and counterstained in 1% uranyl acetate in MQ for 30 minutes in the dark. Thereafter, dehydration was done in a serial dilution of ethanol from 50%, 70%, 90%, 95% to 100%. Sections were further dehydrated in propylene oxide (Sigma Aldrich) and incubated dipped in durcupan resin O/N. On the next day, sections were flat embedded onto silicon coated glass slides and covered with an ACLAR® fluoropolymer film before polymerizing the resin for 2 O/N at 60 °C. Afterwards, rostral/central nuclei of IPN were cut by surgery blade and were re-embedded in resin in a TAAB tube. The resin was polymerized for 2 O/N at 60 °C. 70 nm sections were cut by Leica EM UC7 ultramicrotome (Leica, Germany) and were observed in a Tecnai 12 transmission electron microscope.

Flash and Fix

200–µm thick coronal IPN slices of ChAT-ChR2-EYFP mice were prepared and recovered as described for “Flash and Freeze” experiments. After recovery, slices were incubated for 10 – 15 min in ACSF containing either 2.5 mM Ca^{2+} (“Control” and “10 Hz” groups) or 2.5 mM Ca^{2+} and 1 µM baclofen (“10 Hz + Baclofen” group). Each slice was then optogenetically stimulated three times at 10 Hz for 3 s (10 s interval) followed by immediate immersion fixation in 0.1 M PB containing 4% PFA, 0.05% glutaraldehyde and 15% picric acid under constant agitation for 45 min, followed by washing in 0.1 M PB. Control slices were immersion-fixed without light stimulation. Thereafter, pre-embedding immunolabeling and EM sample preparation was performed as described above.

Analysis

Electrophysiology: All electrophysiological recordings were analyzed in Clampfit (Molecular Devices), Excel (Microsoft, Redmond, WA, USA) and Prism 8 (Graphpad, San Diego, CA, USA).

Flash and Freeze: Serial EM images were analyzed manually in Reconstruct software (John C. Fiala, Ph.D.). The average number of serial images analyzed per synapse was 6.3 ± 0.3 (n=52 synapses). SV diameter was measured in SVs with a clearly visible lipid bilayer as the distance between the two outer membranes through the SV center. The AZ was determined by 1) the presence of a postsynaptic density on the opposing postsynaptic side and 2) electron density inside the synaptic cleft. To minimize variability caused by different synapse sizes, distance of SVs was measured in a specified perimeter around the AZ. Specifically, a box was drawn including the AZ with the following specifications: 150 nm to the left and right of the AZ along the membrane and from there, 200 nm at right angle away from the presynaptic membrane towards the presynaptic cytosol. The open ends were connected to close the box. Inside this box, the distance of the center of all SVs to the closest inner membrane leaflet of the AZ was measured. SVs were considered docked when they had direct

730 contact with the AZ and/or the center of the SV was within a distance of 20–nm to the inner
731 leaflet of the presynaptic membrane.

732 Calcium imaging: Recorded image series were analyzed using Fiji for Image J. In each
733 recording, 3 – 5 puncta were chosen as regions of interest (ROI) and fluorescence was
734 measured at each ROI. Measured values were then normalized to the fluorescence intensity
735 prior to the start of electrical stimulation at each ROI (F_0). For each slice, the time courses of
736 fluorescence intensity at each ROI were then averaged for baseline and baclofen groups,
737 resulting in a single trace for each condition.

738 Flash and Fix: Ultrathin sections of chemically fixed acute slices were analyzed in
739 Reconstruct software to count the number of silver-intensified gold particles in the AZ.

740 Flash and Freeze-fracture: Replica immunogold labeling were analyzed using Darea
741 software[53]. In brief, presynaptic membrane profiles were manually demarcated and gold
742 particles were automatically detected. Validity of automated detection was manually
743 confirmed. Analysis of nearest neighbor distances (NNDs) from 10 nm particles for CAPS2 to
744 the nearest 5 nm particle for SPO were computed to evaluate co-localization of CAPS2 and
745 SPO. We performed Monte-Carlo fitted simulations[53] to place randomly the SPO particles with
746 constraints that they keep the minimum distance of 10 nm to other particles and that the
747 distribution of NND for SPO between the simulated and original particles should not
748 significantly differ (as assessed by two-sample Kolmogorov-Smirnov (KS) test, $p > 0.1$)[53].
749 Statistical differences in NND between CAPS2 to the original and simulated SPO particles
750 were compared by KS test using R software (version 4.1.0).

751 Unless otherwise noted, all data are presented as mean ± SEM. Parametric tests were
752 performed unless data failed Shapiro-Wilk normality test, in which case nonparametric tests
753 were used. Statistical analysis was performed in Prism 8 unless otherwise stated. Figures
754 were prepared using Prism 8 and Photoshop (Adobe, San Jose, CA, USA).

755

Acknowledgments

We thank Erwin Neher and Ipe Ninan for critical comments on the manuscript. This project has received funding from the European Research Council (ERC) and European Commission (EC), under the European Union's Horizon 2020 research and innovation programme (ERC grant agreement no. 694539 to Ryuichi Shigemoto and the Marie Skłodowska-Curie grant agreement no. 665385 to Cihan Önal). This study was supported by the Cooperative Study Program (e－201) of Center for Animal Resources and Collaborative Study of NINS. We thank Kohgaku Eguchi for statistical analysis, Todor Asenov from the ISTA machine shop for custom part preparations for high-pressure freezing and the electron microscopy facility at ISTA for technical support.

Author contributions:

PK performed electrophysiology experiments, calcium imaging, and high-pressure freezing of "Flash and Freeze" and "Flash and Freeze-fracture" experiments; PK and PB fractured "Flash and Freeze-fracture" samples; PB performed immunolabelings for fluorescence imaging, pre-embedding and "Flash and Freeze-fracture" replica sample preparations, and freeze substitution experiments. PB and ELM performed confocal imaging; CÖ performed viral injections, established calcium imaging and cut acute slices for calcium imaging; PK, PB and ELM performed EM imaging of "Flash and Freeze" samples; PK performed "Flash and Freeze-fracture" and "Flash and Fix" EM imaging; YN performed modeling based on calcium imaging data; CBM taught PK how to use Leica EM ICE; MS and MH made SPO KO mice using the CRISPR/Cas9 method; PJ, NB and TS provided tools and reagents. PK analyzed data and prepared figures; RS and PK conceived the study, designed experiments, and wrote the manuscript. All authors have read and jointly revised the manuscript and approved its content.

References

1 Bhandari, P. *et al.* $GABA_B$ receptor auxiliary subunits modulate Cav2.3-mediated release from medial habenula terminals. *Elife* **10**, doi:10.7554/eLife.68274 (2021).

2 Koppensteiner, P., Galvin, C. & Ninan, I. Development- and experience-dependent plasticity in the dorsomedial habenula. *Mol Cell Neurosci* **77**, 105-112, doi:10.1016/j.mcn.2016.10.006 (2016).

3 Koppensteiner, P., Melani, R. & Ninan, I. A Cooperative Mechanism Involving Ca^{2+}-Permeable AMPA Receptors and Retrograde Activation of $GABA_B$ Receptors in Interpeduncular Nucleus Plasticity. *Cell Rep* **20**, 1111-1122, doi:10.1016/j.celrep.2017.07.013 (2017).

4 Zhang, J. *et al.* Presynaptic Excitation via GABAB Receptors in Habenula Cholinergic Neurons Regulates Fear Memory Expression. *Cell* **166**, 716-728, doi:10.1016/j.cell.2016.06.026 (2016).

5 Gassmann, M. & Bettler, B. Regulation of neuronal GABA(B) receptor functions by subunit composition. *Nat Rev Neurosci* **13**, 380-394, doi:10.1038/nrn3249 (2012).

6 Melani, R., Von Itter, R., Jing, D., Koppensteiner, P. & Ninan, I. Opposing effects of an atypical glycinergic and substance P transmission on interpeduncular nucleus plasticity. *Neuropsychopharmacology* **44**, 1828-1836, doi:10.1038/s41386-019-0396-6 (2019).

7 Fioravante, D. & Regehr, W. G. Short-term forms of presynaptic plasticity. *Curr Opin Neurobiol* **21**, 269-274, doi:10.1016/j.conb.2011.02.003 (2011).

8 Neher, E. & Brose, N. Dynamically Primed Synaptic Vesicle States: Key to Understand Synaptic Short-Term Plasticity. *Neuron* **100**, 1283-1291, doi:10.1016/j.neuron.2018.11.024 (2018).

9 Atwood, H. L. & Karunanithi, S. Diversification of synaptic strength: presynaptic elements. *Nat Rev Neurosci* **3**, 497-516, doi:10.1038/nrn876 (2002).

10 Zucker, R. S. & Regehr, W. G. Short-term synaptic plasticity. *Annu Rev Physiol* **64**, 355-405, doi:10.1146/annurev.physiol.64.092501.114547 (2002).

11 Aldahabi, M. *et al.* Different priming states of synaptic vesicles underlie distinct release probabilities at hippocampal excitatory synapses. *Neuron*, doi:10.1016/j.neuron.2022.09.035 (2022).

12 Zhao, H. & Rusak, B. Circadian firing-rate rhythms and light responses of rat habenular nucleus neurons in vivo and in vitro. *Neuroscience* **132**, 519-528, doi:10.1016/j.neuroscience.2005.01.012 (2005).

13 Sharp, P. E., Turner-Williams, S. & Tuttle, S. Movement-related correlates of single cell activity in the interpeduncular nucleus and habenula of the rat during a pellet-chasing task. *Behav Brain Res* **166**, 55-70, doi:10.1016/j.bbr.2005.07.004 (2006).

14 Sylwestrak, E. L. *et al.* Cell-type-specific population dynamics of diverse reward computations. *Cell* **185**, 3568-3587 e3527, doi:10.1016/j.cell.2022.08.019 (2022).

15 Ren, J. *et al.* Habenula "cholinergic" neurons co-release glutamate and acetylcholine and activate postsynaptic neurons via distinct transmission modes. *Neuron* **69**, 445-452, doi:10.1016/j.neuron.2010.12.038 (2011).

16 Kalkstein, J. M. & Magleby, K. L. Augmentation increases vesicular release probability in the presence of masking depression at the frog neuromuscular junction. *J Neurosci* **24**, 11391-11403, doi:10.1523/JNEUROSCI.2756-04.2004 (2004).

17 Eggermann, E., Bucurenciu, I., Goswami, S. P. & Jonas, P. Nanodomain coupling between Ca(2)(+) channels and sensors of exocytosis at fast mammalian synapses. *Nat Rev Neurosci* **13**, 7-21, doi:10.1038/nrn3125 (2011).

18 Schneggenburger, R., Meyer, A. C. & Neher, E. Released fraction and total size of a pool of immediately available transmitter quanta at a calyx synapse. *Neuron* **23**, 399-409, doi:10.1016/s0896-6273(00)80789-8 (1999).

19 Kaeser, P. S. & Regehr, W. G. The readily releasable pool of synaptic vesicles. *Curr Opin Neurobiol* **43**, 63-70, doi:10.1016/j.conb.2016.12.012 (2017).

20 Imig, C. *et al.* The morphological and molecular nature of synaptic vesicle priming at presynaptic active zones. *Neuron* **84**, 416-431, doi:10.1016/j.neuron.2014.10.009 (2014).

21 Borges-Merjane, C., Kim, O. & Jonas, P. Functional Electron Microscopy, "Flash and Freeze," of Identified Cortical Synapses in Acute Brain Slices. *Neuron* **105**, 992-1006 e1006, doi:10.1016/j.neuron.2019.12.022 (2020).

22 Nagel, G. *et al.* Channelrhodopsin-2, a directly light-gated cation-selective membrane channel. *Proc Natl Acad Sci U S A* **100**, 13940-13945, doi:10.1073/pnas.1936192100 (2003).

23 Berndt, A. *et al.* High-efficiency channelrhodopsins for fast neuronal stimulation at low light levels. *Proc Natl Acad Sci U S A* **108**, 7595-7600, doi:10.1073/pnas.1017210108 (2011).

24 Knaus, P., Marqueze-Pouey, B., Scherer, H. & Betz, H. Synaptoporin, a novel putative channel protein of synaptic vesicles. *Neuron* **5**, 453-462, doi:10.1016/0896-6273(90)90084-s (1990).

25 Singec, I. *et al.* Synaptic vesicle protein synaptoporin is differently expressed by subpopulations of mouse hippocampal neurons. *J Comp Neurol* **452**, 139-153, doi:10.1002/cne.10371 (2002).

26 Müller, C. S. *et al.* Quantitative proteomics of the Cav2 channel nano-environments in the mammalian brain. *Proc Natl Acad Sci U S A* **107**, 14950-14957, doi:10.1073/pnas.1005940107 (2010).

27 Jockusch, W. J. *et al.* CAPS-1 and CAPS-2 are essential synaptic vesicle priming proteins. *Cell* **131**, 796-808, doi:10.1016/j.cell.2007.11.002 (2007).

28 Sadakata, T. *et al.* Impaired cerebellar development and function in mice lacking CAPS2, a protein involved in neurotrophin release. *J Neurosci* **27**, 2472-2482, doi:10.1523/JNEUROSCI.2279-06.2007 (2007).

29 Shinoda, Y. *et al.* Calcium-dependent activator protein for secretion 2 (CAPS2) promotes BDNF secretion and is critical for the development of GABAergic interneuron network. *Proc Natl Acad Sci U S A* **108**, 373-378, doi:10.1073/pnas.1012220108 (2011).

30 Sadakata, T. *et al.* Differential distributions of the Ca2+ -dependent activator protein for secretion family proteins (CAPS2 and CAPS1) in the mouse brain. *J Comp Neurol* **495**, 735-753, doi:10.1002/cne.20947 (2006).

31 Lin, K. H., Taschenberger, H. & Neher, E. A sequential two-step priming scheme reproduces diversity in synaptic strength and short-term plasticity. *Proc Natl Acad Sci U S A* **119**, e2207987119, doi:10.1073/pnas.2207987119 (2022).

32 Neher, E. & Taschenberger, H. Non-negative Matrix Factorization as a Tool to Distinguish Between Synaptic Vesicles in Different Functional States. *Neuroscience* **458**, 182-202, doi:10.1016/j.neuroscience.2020.10.012 (2021).

33 Sadakata, T. *et al.* The secretory granule-associated protein CAPS2 regulates neurotrophin release and cell survival. *J Neurosci* **24**, 43-52, doi:10.1523/JNEUROSCI.2528-03.2004 (2004).

34 Berwin, B., Floor, E. & Martin, T. F. CAPS (mammalian UNC-31) protein localizes to membranes involved in dense-core vesicle exocytosis. *Neuron* **21**, 137-145, doi:10.1016/s0896-6273(00)80521-8 (1998).

35 Stevens, D. R. & Rettig, J. The Ca(2+)-dependent activator protein for secretion CAPS: do I dock or do I prime? *Mol Neurobiol* **39**, 62-72, doi:10.1007/s12035-009-8052-5 (2009).

36 Nguyen Truong, C. Q. *et al.* Secretory vesicle priming by CAPS is independent of its SNARE-binding MUN domain. *Cell Rep* **9**, 902-909, doi:10.1016/j.celrep.2014.09.050 (2014).

37 Vandael, D., Borges-Merjane, C., Zhang, X. & Jonas, P. Short-Term Plasticity at Hippocampal Mossy Fiber Synapses Is Induced by Natural Activity Patterns and Associated with Vesicle Pool Engram Formation. *Neuron* **107**, 509-521 e507, doi:10.1016/j.neuron.2020.05.013 (2020).

38 Maciewicz, R., Foote, W. E. & Bry, J. Excitatory projection from the interpeduncular nucleus to central superior raphe neurons. *Brain Res* **225**, 179-183, doi:10.1016/0006-8993(81)90327-9 (1981).

878 39 Marcinkiewicz, M., Morcos, R. & Chretien, M. CNS connections with the median raphe
879 nucleus: retrograde tracing with WGA-apoHRP-Gold complex in the rat. *J Comp Neurol* **289**,
880 11-35, doi:10.1002/cne.902890103 (1989).
881 40 McLaughlin, I., Dani, J. A. & De Biasi, M. The medial habenula and interpeduncular nucleus
882 circuitry is critical in addiction, anxiety, and mood regulation. *J Neurochem* **142 Suppl 2**, 130-
883 143, doi:10.1111/jnc.14008 (2017).
884 41 Szonyi, A. *et al.* Median raphe controls acquisition of negative experience in the mouse.
885 *Science* **366**, eaay8746, doi:10.1126/science.aay8746 (2019).
886 42 Varga, V., Kekesi, A., Juhasz, G. & Kocsis, B. Reduction of the extracellular level of glutamate
887 in the median raphe nucleus associated with hippocampal theta activity in the anaesthetized
888 rat. *Neuroscience* **84**, 49-57, doi:10.1016/s0306-4522(97)00489-2 (1998).
889 43 Viana Di Prisco, G., Albo, Z., Vertes, R. P. & Kocsis, B. Discharge properties of neurons of the
890 median raphe nucleus during hippocampal theta rhythm in the rat. *Exp Brain Res* **145**, 383-
891 394, doi:10.1007/s00221-002-1123-8 (2002).
892 44 Bromberg-Martin, E. S., Matsumoto, M. & Hikosaka, O. Distinct tonic and phasic anticipatory
893 activity in lateral habenula and dopamine neurons. *Neuron* **67**, 144-155,
894 doi:10.1016/j.neuron.2010.06.016 (2010).
895 45 Yoo, H. *et al.* Down-regulation of habenular calcium-dependent secretion activator 2 induces
896 despair-like behavior. *Sci Rep* **11**, 3700, doi:10.1038/s41598-021-83310-0 (2021).
897 46 Kawaja, M. D., Flumerfelt, B. A. & Hrycyshyn, A. W. Glutamate decarboxylase
898 immunoreactivity in the rat interpeduncular nucleus: a light and electron microscope
899 investigation. *Neuroscience* **30**, 741-753, doi:10.1016/0306-4522(89)90166-8 (1989).
900 47 Kawaja, M. D., Flumerfelt, B. A. & Hrycyshyn, A. W. Simultaneous demonstration of choline
901 acetyltransferase and glutamic acid decarboxylase immunoreactivity in the rat
902 interpeduncular nucleus. *J Chem Neuroanat* **3**, 165-177 (1990).
903 48 Antolin-Fontes, B., Ables, J. L., Gorlich, A. & Ibanez-Tallon, I. The habenulo-interpeduncular
904 pathway in nicotine aversion and withdrawal. *Neuropharmacology* **96**, 213-222,
905 doi:10.1016/j.neuropharm.2014.11.019 (2015).
906 49 Adams, D. J., Arthur, C. P. & Stowell, M. H. Architecture of the Synaptophysin/Synaptobrevin
907 Complex: Structural Evidence for an Entropic Clustering Function at the Synapse. *Sci Rep* **5**,
908 13659, doi:10.1038/srep13659 (2015).
909 50 Nakamura, Y. *et al.* Nanoscale distribution of presynaptic Ca(2+) channels and its impact on
910 vesicular release during development. *Neuron* **85**, 145-158,
911 doi:10.1016/j.neuron.2014.11.019 (2015).
912 51 Li, L., Bischofberger, J. & Jonas, P. Differential gating and recruitment of P/Q-, N-, and R-type
913 Ca2+ channels in hippocampal mossy fiber boutons. *J Neurosci* **27**, 13420-13429,
914 doi:10.1523/JNEUROSCI.1709-07.2007 (2007).
915 52 Sheng, J. *et al.* Calcium-channel number critically influences synaptic strength and plasticity at
916 the active zone. *Nat Neurosci* **15**, 998-1006, doi:10.1038/nn.3129 (2012).
917 53 Kleindienst, D. *et al.* Deep Learning-Assisted High-Throughput Analysis of Freeze-Fracture
918 Replica Images Applied to Glutamate Receptors and Calcium Channels at Hippocampal
919 Synapses. *Int J Mol Sci* **21**, doi:10.3390/ijms21186737 (2020).

920

921

Figure Legends

Figure 1: Stimulation of MHb axons at a physiological frequency reveals transition from tonic to phasic neurotransmitter release by baclofen

A Scheme of the 1 mm thick angled slice preparation (top) and an example of the recording configuration in the resulting slice (bottom). **B** Example traces of EPSCs evoked by 10–Hz stimulation in one cell before and after the application of baclofen. Greyed responses represent individual sweeps, and bold responses represent the average of the individual traces. **C** Quantification of baseline and baclofen responses using cumulative EPSC amplitudes. **D** Plot of EPSC responses after normalization of EPSC amplitudes to the amplitude of the corresponding first baseline EPSC **E** Overlay of 7 traces of 10 Hz responses at baseline and during baclofen in one cell with single stimulations at varying intervals following the 10 Hz stimulus. **F** Overlay of single stimuli color-coded with stimulation time. **G** Quantification of recovery from tonic release augmentation and phasic release depletion. Using exponential fit, both short-term plasticity exhibited recovery times in the order of seconds.

See also Extended Data Fig. 1

Figure 2: Role of presynaptic Ca^{2+} in tonic and phasic neurotransmission

A Example images of axon-GCaMP6s fluorescence at rest (left) and at peak fluorescence during stimulation (middle) under baseline (top) and baclofen conditions (bottom). Subtraction of resting fluorescence from peak fluorescence reveals stimulation-induced fluorescence in a subset of MHb axons (right panels). Scale bars, 50 µm **B** Quantification of GCaMP6s fluorescence time course during stimulation under baseline and baclofen conditions in five slices from five mice. *** $P < 0.001$ two-way ANOVA with Bonferroni post hoc test **C** Example traces of 10–Hz responses at 2.5 mM and 5 mM Ca^{2+} and at 5 mM Ca^{2+} + 1 µM baclofen. **D** Cumulative EPSC amplitude quantification reveals tonic release at 5 mM Ca^{2+} and a strong

transition to phasic release after the addition of baclofen. **E** Normalization of EPSC responses to the first EPSC in the train shows augmentation in 2.5 and 5 mM Ca^{2+} condition and depletion at 5 mM Ca^{2+} + baclofen. **F – G** K^+ channel blockers TEA and 4-AP did not induce phasic release and did not occlude phasic release induction by baclofen. **I** Example trace of a phasic response before and 10 min after the application of 100 µM EGTA-AM. **J** Cumulative EPSC amplitude plot before and after EGTA-AM application. **K** Comparison before and after EGTA-AM application reveals significant reduction in $EPSC_1$ amplitude. P value calculated with Wilcoxon test. **L – N** Application of EGTA-AM prior to baclofen prevents phasic release induction but does not significantly alter tonic release and its $EPSC_1$ amplitudes. P value calculated by one-way ANOVA.

See also Extended Data Fig. 2 and Extended Data Table 1

Figure 3: Comparison of RRP and P_r between tonic and phasic release

A Example traces of EPSC responses during 100–Hz stimulation at baseline and after baclofen application. **B** Baseline and baclofen cumulative EPSC amplitude plots with linear regression fit through the last 6 stimuli (#25 – #30). **C** Paired comparison of RRP sizes before and after baclofen. P value derived from Wilcoxon t-test. **D** Paired comparison of P_r at baseline and after baclofen, P values calculated by two-tailed unpaired t-test.

Figure 4: Structural correlates of enhanced neurotransmitter release

A EYFP Fluorescence in an angled ChAT-ChR2-EYFP slice (left) and tonic and phasic example traces evoked by optogenetic stimulation in a cell before and during the application of baclofen. **B** Recovery time courses of normalized EPSC amplitudes after augmentation (baseline) and depletion (baclofen). **C** Top, expanded phasic example trace from panel A highlighting freezing time points for depletion and recovery groups in the presence of baclofen.

Bottom left, overlay of individual EPSCs over the course of recovery. Bottom right, overlay of individual EPSC onsets during phasic release recovery. **D** Step-by-step scheme displaying the “Flash and Freeze” experiments up to the freezing step. **E** Example EM images of synapses from Control, Depletion and Recovery groups. Scale bars, 100 nm **F** Quantification of synaptic vesicle (SV) diameters across groups. P value derived from one-way ANOVA. **G** Plot of SV numbers (normalized to the number of analyzed serial sections) in bins of 5–nm from the AZ membrane. *** $P < 0.001$ Recovery vs. Control and Depletion, two-way ANOVA with Bonferroni post hoc test. **H** Quantification of docked SV densities. Values above bars indicate p values calculated by one-way ANOVA with Tukey post hoc test.

See also Extended Data Fig. 3

Figure 5: SV-associated molecules involved in tonic and phasic neurotransmitter release

A Confocal images of anti-synaptoporin immunofluorescence labeling in the IPN of a WT and a SPO KO mouse. Scale bars, 100 µm. **B** Pre-embedding immunolabeling for SPO in an MHb terminal, showing gold particles co-localized with SVs. Scale bar, 100 nm. **C** Example 10–Hz EPSC traces of a recording in an acute slice from a SPO KO mouse at baseline and during baclofen application. **D** Tonic release augmentation was significantly impaired in SPO KO mice, displayed P value of main effect of genotype, calculated by two-way ANOVA. Bonferroni post hoc analysis revealed a significant difference in stimuli #20 – #30. **E** Overlay of phasic release P_r time course between WT and SPO KO mice, calculated by linear regression analysis of cumulative EPSC amplitude plots[18]. **F** P_r of $EPSC_1$ in the phasic response train was not different between WT and SPO KO mice. P value calculated from two-tailed unpaired t-test. **G** Confocal images of anti-CAPS2 immunofluorescence labeling in the IPN of a WT and CAPS2 KO mouse. Scale bars, 100 µm **H** Pre-embedding immunolabeling for CAPS2 in a MHb terminal shows gold particles co-localized with SVs. Scale bar, 100 nm. **I** Example 10 Hz

EPSC traces recorded in an acute slice from a CAPS2 KO mouse at baseline and during baclofen application. **J** Augmentation remained unaffected by genetic ablation of CAPS2. Main effect of genotype P value calculated via two-way ANOVA **K** P_r time course of phasic release, calculated by linear regression analysis of cumulative EPSC amplitude plots, was strongly affected by genetic ablation of CAPS2 compared to WT. **L** P_r of $EPSC_1$ in the phasic response was significantly lower in CAPS2 KO compared to WT mice. P value calculated by two-tailed unpaired t-test.

See also Extended Data Fig. 4 and Extended Data Fig. 5

Figure 6: Potentiation by GBR activation and its storage is activity-dependent

A Example thick-slice configuration of recording in IPN with bilateral MHb input stimulation. To examine activity-dependence (**B**), a single IPN neuron was patched and after bilateral baseline recordings (10–Hz stimulation for 3 s, 5–s interval between left and right side stimulations, 20 s between sweeps), stimulation with the red-highlighted electrode was halted during baclofen washin, whereas stimulation was continued with the other electrode (10 Hz, 3–s duration, every 20 s). Once maximal potentiation was reached, stimulation with the red-highlighted electrode resumed. To examine storage of potentiation (**C**), after bilateral baseline recording and bilateral induction of maximal potentiation, baclofen washout commenced and stimulation with the red-highlighted electrode was halted. Stimulation with the other electrode continued and, once potentiation was fully reverted, stimulation with the red-highlighted electrode resumed. **B** Left, example traces derived from the silent side at baseline (1), at the first (2) and second (3) 10–Hz stimulus after silent baclofen washin. Right, time course of $EPSC_1$ amplitudes, relative to baseline, during stimulated and silent washin of baclofen. **C** Left, example traces derived from the silent side at peak potentiation (1), at the first (2) and second (3) stimulus after silent baclofen washout. Right, time course of relative $EPSC_1$ amplitudes during stimulated and silent washout of baclofen.

Figure 7: Recruitment of CAPS2 to the active zone during phasic release

A Example images of pre-embedding EM labeling for CAPS2 in acute slices under control conditions without stimulation and after 10–Hz stimulation in the absence (10 Hz) or presence of 1 µM baclofen (10 Hz + Baclofen). **B** Quantification of particle numbers in the AZ reveals significantly larger CAPS2 particle numbers in the "10 Hz + Baclofen" group compared to the other groups. P values calculated by one-way ANOVA with Tukey post hoc test.

Figure 8: "Flash and Freeze-fracture" replica immunolabeling for SPO and CAPS2 in the presynaptic active zone during tonic and phasic release

A "Flash and Freeze-fracture" steps schematic. Left Panel, "Flash and Freeze" of acute brain slices using sapphire/metal hybrid sandwich separated by a double-sided tape. Middle panel, Freeze-fracture replication of frozen brain slices using a knife to separate sapphire from the metal carrier. Right Panel, SDS treatment of tissue and immunolabeling with primary antibodies against SPO and CAPS2 followed by labeling with 5 nm and 10 nm gold-conjugated secondary antibodies. **B** Example images of SPO and CAPS2 labeling in "Flash and Freeze-fracture" replicas frozen without light stimulation (ACSF) or after an 8 ms light pulse in the absence (Stimulation) or presence of 1 µM baclofen (Stimulation + Baclofen). Scale bars, 100 nm **C** Quantification of CAPS2/SPO particle ratio revealed a significant increase in the "Stimulation + Baclofen" group. P values derived from one-way ANOVA with Tukey post hoc test. **D** Summary scheme depicting a hypothetical two-pool mechanism underlying the transition from the tonic to phasic release mode in MHb terminals. Left: In the basal release condition, tonic SPO-positive SVs are loosely docked in close vicinity of Cav2.3, whereas CAPS2-positive phasic SVs are located more distally and undocked. Action potential-triggered Ca^{2+} influx is small and only closely located SPO-positive tonic SVs fuse with the AZ membrane. Right: In the enhanced release condition, GBR activation coupled with action

potential-mediated depolarization produces a massive influx of Ca^{2+}, which initially triggers release of closely located SPO-positive tonic SVs but also rapidly recruits larger number of distal CAPS2-positive phasic SVs (middle) to the AZ. The subsequent action potentials trigger the release of both closely located tonic and newly recruited phasic SVs, resulting in an increased RRP (right). Following the fusion of CAPS2-positive phasic SVs, CAPS2 remains membrane-bound and may act as a docking site for replenished phasic SVs, resulting in retention of the increased RRP.

See also Extended Data Fig. 6

Figure 1

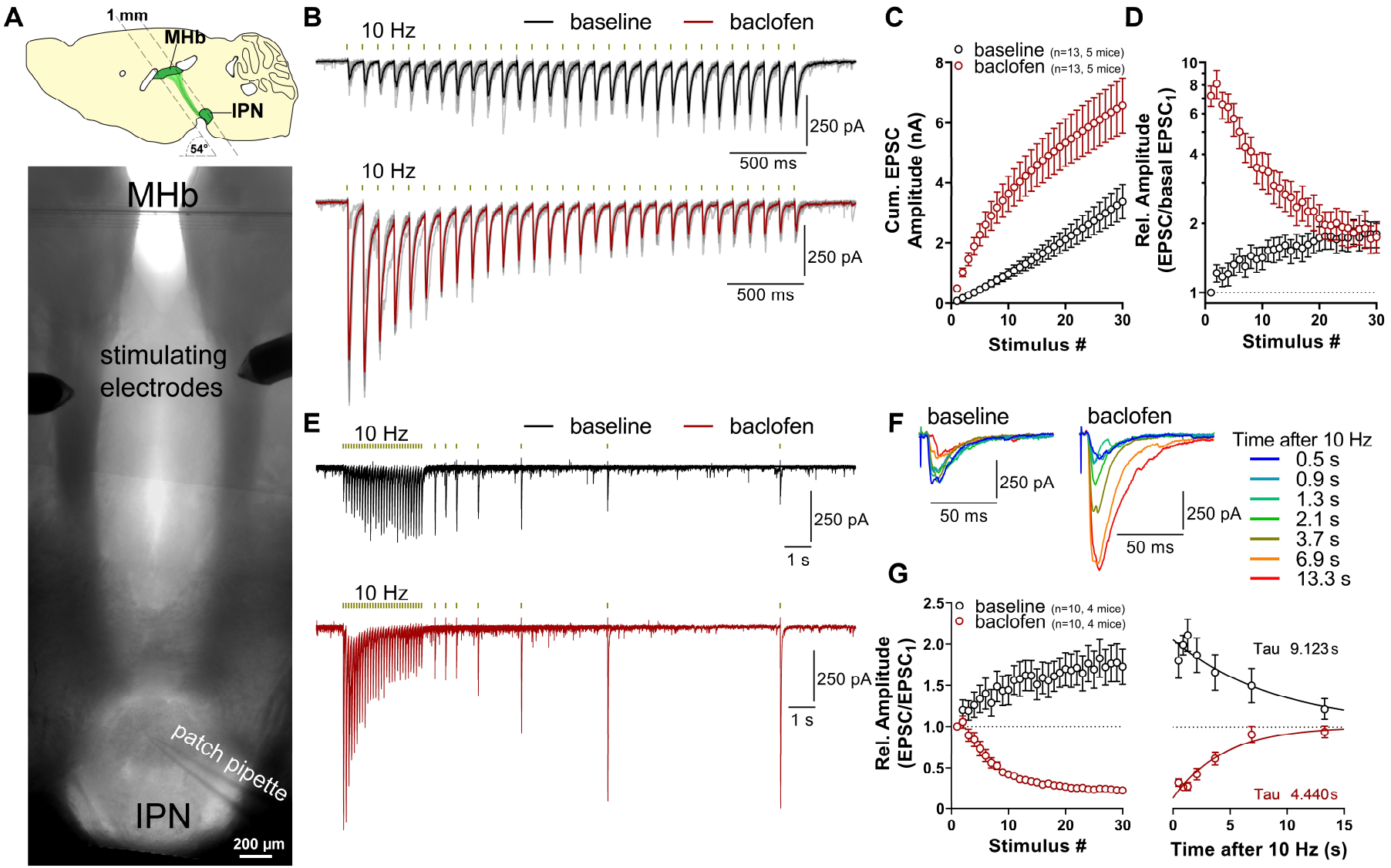
A
1 mm
MHb
IPN
54°
MHb
stimulating electrodes
patch pipette
IPN
200 µm
B
10 Hz
baseline
baclofen
250 pA
500 ms
10 Hz
250 pA
500 ms
C
baseline (n=13, 5 mice)
baclofen (n=13, 5 mice)
Cum. EPSC Amplitude (nA)
Stimulus #
D
Rel. Amplitude (EPSC/basal EPSC1)
Stimulus #
E
10 Hz
baseline
baclofen
250 pA
1 s
10 Hz
250 pA
1 s
F
baseline
baclofen
250 pA
50 ms
250 pA
50 ms
Time after 10 Hz
0.5 s
0.9 s
1.3 s
2.1 s
3.7 s
6.9 s
13.3 s
G
baseline (n=10, 4 mice)
baclofen (n=10, 4 mice)
Rel. Amplitude (EPSC/EPSC1)
Stimulus #
Tau 9.123 s
Tau 4.440 s
Time after 10 Hz (s)

Figure 2

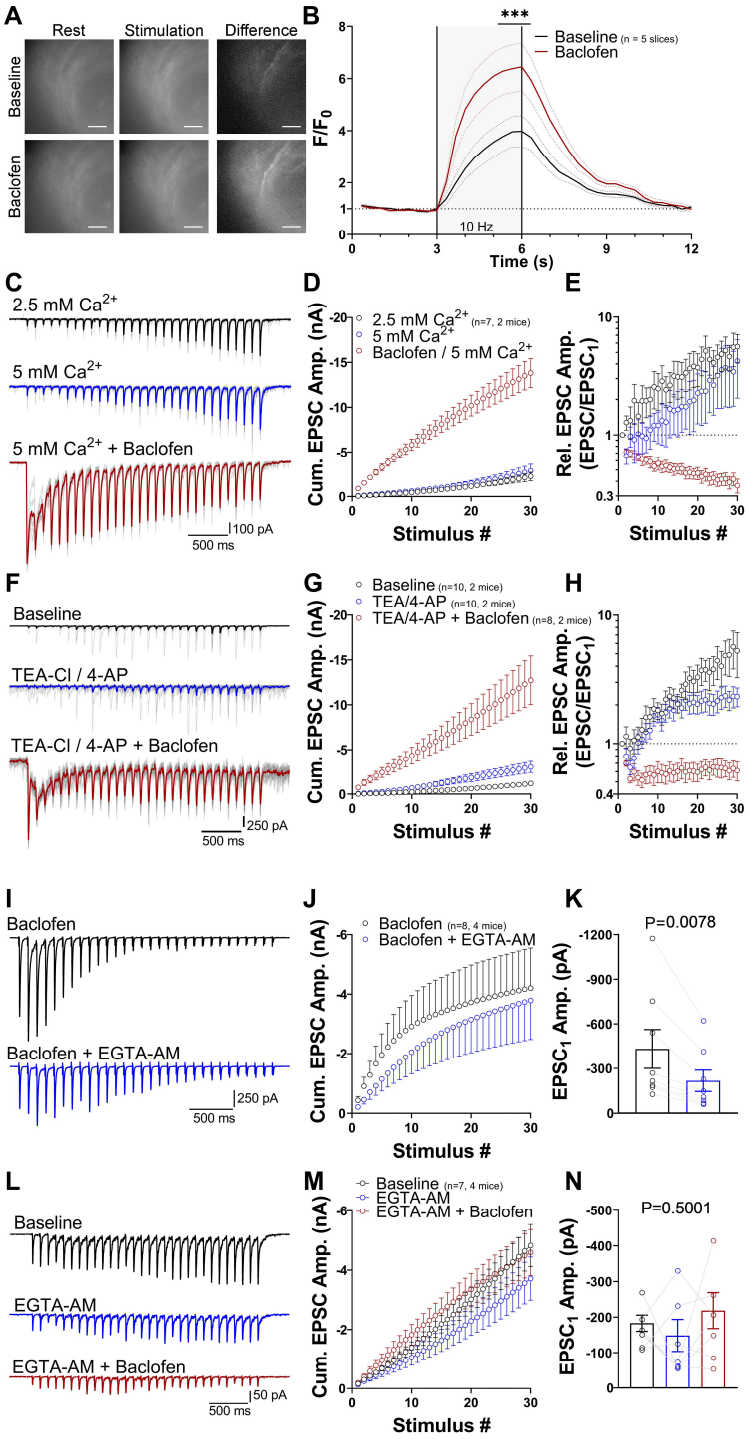
A
Rest
Stimulation
Difference
Baseline
Baclofen
B
***
Baseline (n = 5 slices)
Baclofen
F/F0
10 Hz
Time (s)
C
2.5 mM Ca2+
5 mM Ca2+
5 mM Ca2+ + Baclofen
100 pA
500 ms
D
2.5 mM Ca2+ (n=7, 2 mice)
5 mM Ca2+
Baclofen / 5 mM Ca2+
Cum. EPSC Amp. (nA)
Stimulus #
E
Rel. EPSC Amp. (EPSC/EPSC1)
Stimulus #
F
Baseline
TEA-Cl / 4-AP
TEA-Cl / 4-AP + Baclofen
250 pA
500 ms
G
Baseline (n=10, 2 mice)
TEA/4-AP (n=10, 2 mice)
TEA/4-AP + Baclofen (n=8, 2 mice)
Cum. EPSC Amp. (nA)
Stimulus #
H
Rel. EPSC Amp. (EPSC/EPSC1)
Stimulus #
I
Baclofen
Baclofen + EGTA-AM
250 pA
500 ms
J
Baclofen (n=8, 4 mice)
Baclofen + EGTA-AM
Cum. EPSC Amp. (nA)
Stimulus #
K
P=0.0078
EPSC1 Amp. (pA)
L
Baseline
EGTA-AM
EGTA-AM + Baclofen
50 pA
500 ms
M
Baseline (n=7, 4 mice)
EGTA-AM
EGTA-AM + Baclofen
Cum. EPSC Amp. (nA)
Stimulus #
N
P=0.5001
EPSC1 Amp. (pA)

Figure 3

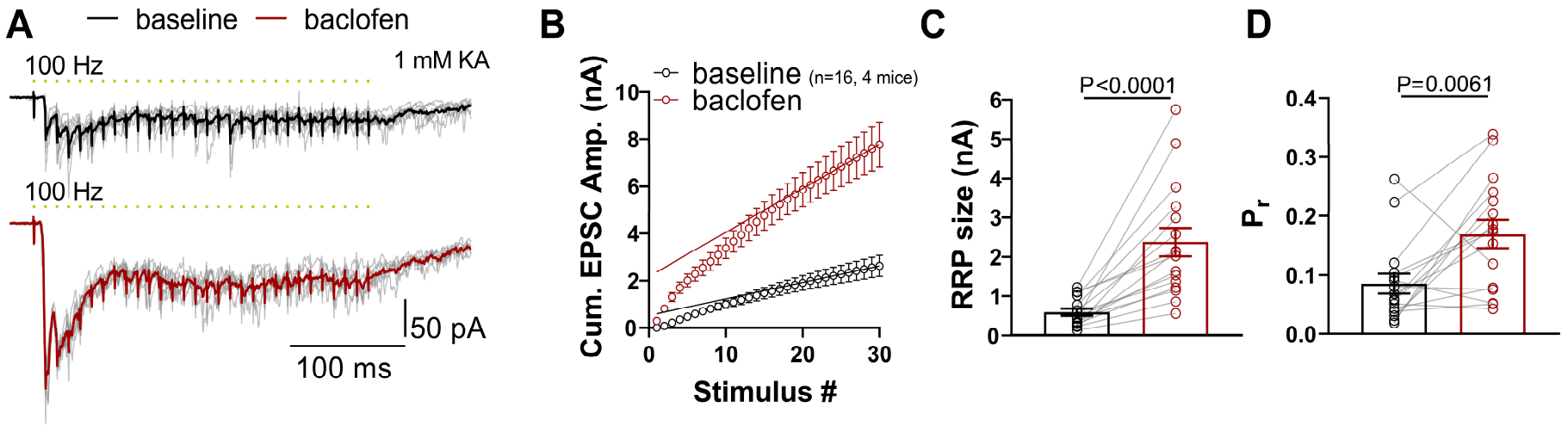
A
baseline
baclofen
100 Hz
1 mM KA
100 Hz
50 pA
100 ms
B
baseline (n=16, 4 mice)
baclofen
Cum. EPSC Amp. (nA)
Stimulus #
C
P<0.0001
RRP size (nA)
D
P=0.0061
Pr

Figure 4

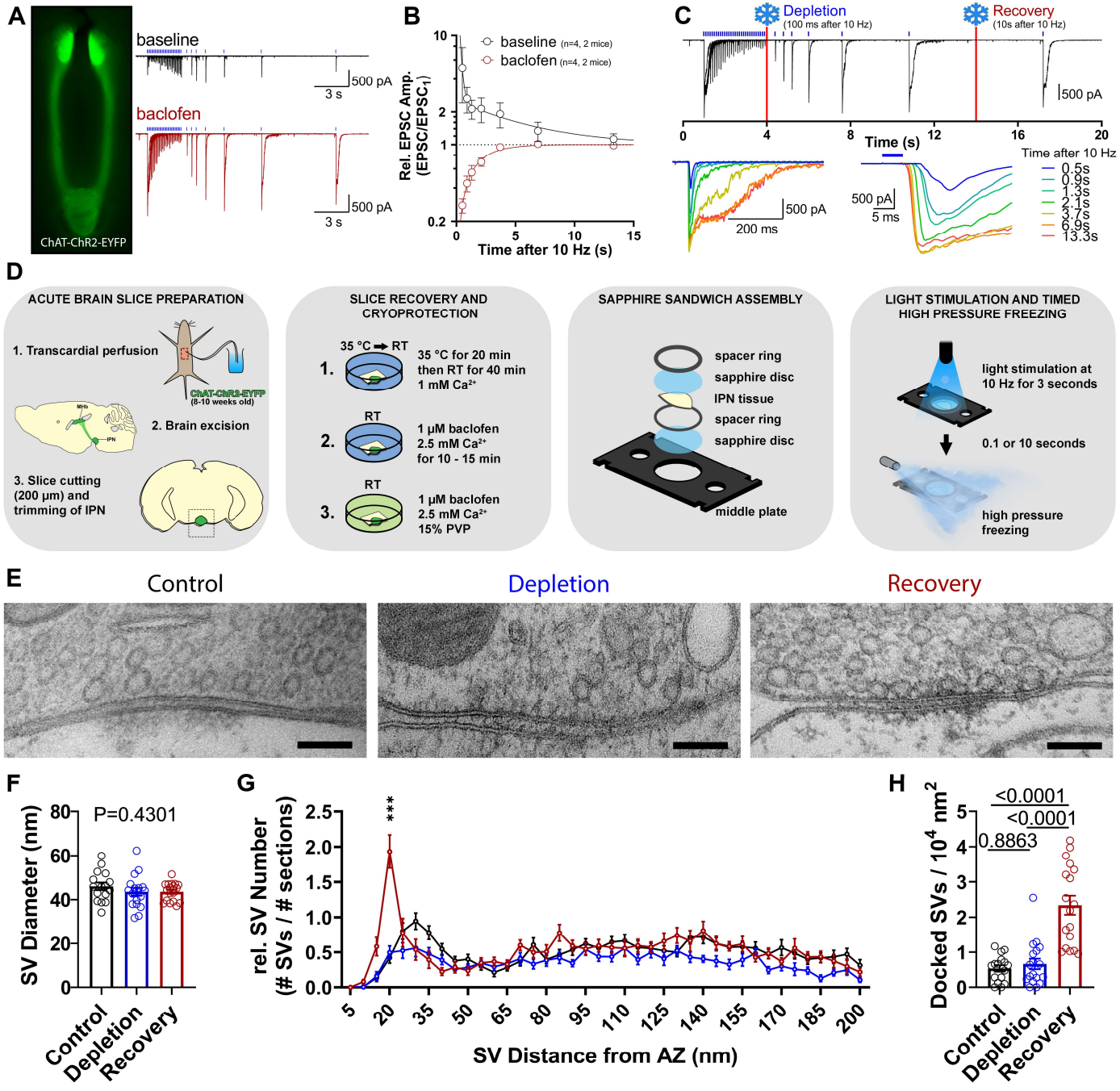
A
baseline
500 pA
3 s
baclofen
500 pA
3 s
ChAT-ChR2-EYFP
B
baseline (n=4, 2 mice)
baclofen (n=4, 2 mice)
Rel. EPSC Amp. (EPSC/EPSC1)
Time after 10 Hz (s)
C
Depletion
(100 ms after 10 Hz)
Recovery
(10s after 10 Hz)
500 pA
Time (s)
Time after 10 Hz
0.5s
0.9s
1.3s
2.1s
3.7s
6.9s
13.3s
500 pA
200 ms
500 pA
5 ms
D
ACUTE BRAIN SLICE PREPARATION
1. Transcardial perfusion
ChAT-ChR2-EYFP
(8-10 weeks old)
2. Brain excision
3. Slice cutting
(200 µm) and
trimming of IPN
SLICE RECOVERY AND
CRYOPROTECTION
35 °C ➡ RT
1. 35 °C for 20 min
then RT for 40 min
1 mM Ca2+
RT
2. 1 µM baclofen
2.5 mM Ca2+
for 10 - 15 min
RT
3. 1 µM baclofen
2.5 mM Ca2+
15% PVP
SAPPHIRE SANDWICH ASSEMBLY
spacer ring
sapphire disc
IPN tissue
spacer ring
sapphire disc
middle plate
LIGHT STIMULATION AND TIMED
HIGH PRESSURE FREEZING
light stimulation at
10 Hz for 3 seconds
0.1 or 10 seconds
high pressure
freezing
E
Control
Depletion
Recovery
F
SV Diameter (nm)
P=0.4301
Control
Depletion
Recovery
G
rel. SV Number
(# SVs / # sections)
***
SV Distance from AZ (nm)
H
Docked SVs / 10^4 nm^2
<0.0001
<0.0001
0.8863
Control
Depletion
Recovery

Figure 5

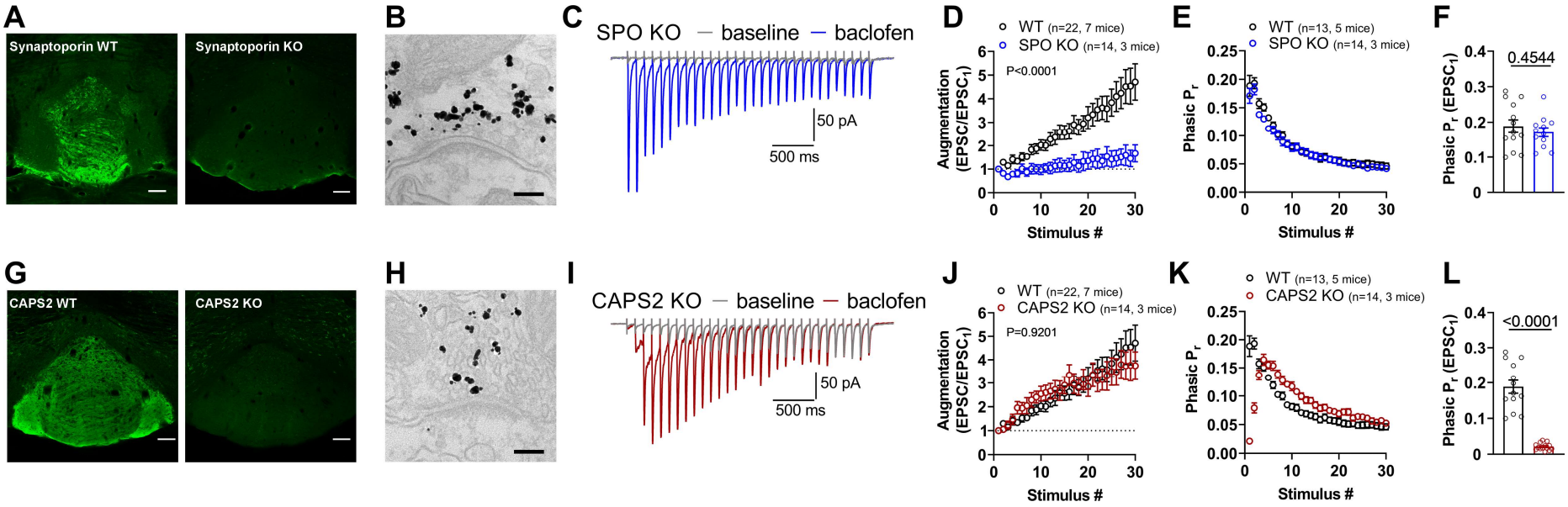
A
Synaptoporin WT
Synaptoporin KO
B
C
SPO KO — baseline — baclofen
50 pA
500 ms
D
WT (n=22, 7 mice)
SPO KO (n=14, 3 mice)
P<0.0001
Augmentation (EPSC/EPSC1)
Stimulus #
E
WT (n=13, 5 mice)
SPO KO (n=14, 3 mice)
Phasic Pr
Stimulus #
F
0.4544
Phasic Pr (EPSC1)
G
CAPS2 WT
CAPS2 KO
H
I
CAPS2 KO — baseline — baclofen
50 pA
500 ms
J
WT (n=22, 7 mice)
CAPS2 KO (n=14, 3 mice)
P=0.9201
Augmentation (EPSC/EPSC1)
Stimulus #
K
WT (n=13, 5 mice)
CAPS2 KO (n=14, 3 mice)
Phasic Pr
Stimulus #
L
<0.0001
Phasic Pr (EPSC1)

Figure 6

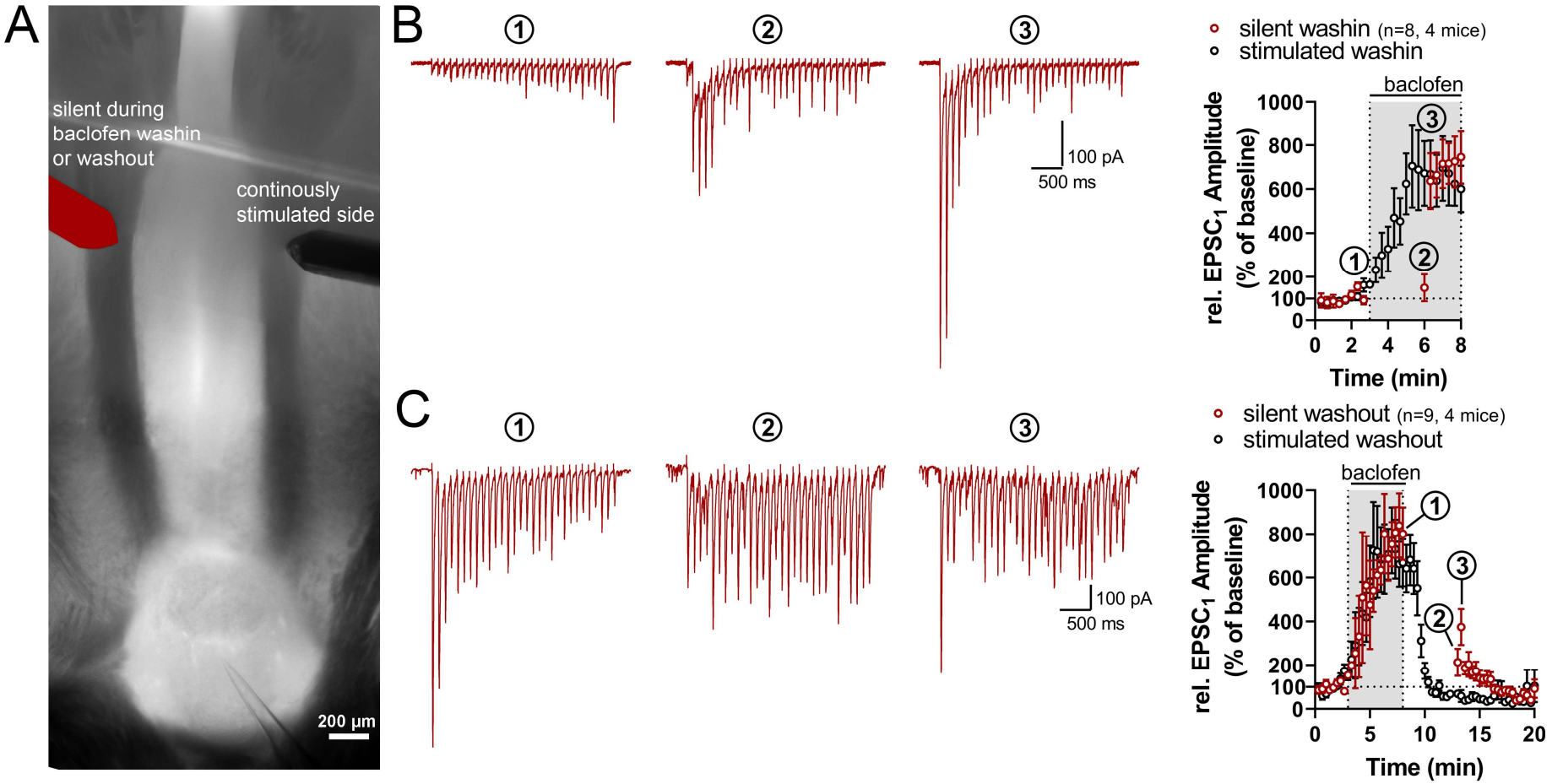
A
silent during
baclofen washin
or washout
continously
stimulated side
200 µm
B
①
②
③
100 pA
500 ms
C
①
②
③
100 pA
500 ms
silent washin (n=8, 4 mice)
stimulated washin
baclofen
rel. EPSC1 Amplitude
(% of baseline)
1000
800
600
400
200
100
0
0
2
4
6
8
Time (min)
silent washout (n=9, 4 mice)
stimulated washout
baclofen
rel. EPSC1 Amplitude
(% of baseline)
1000
800
600
400
200
100
0
0
5
10
15
20
Time (min)

Figure 7

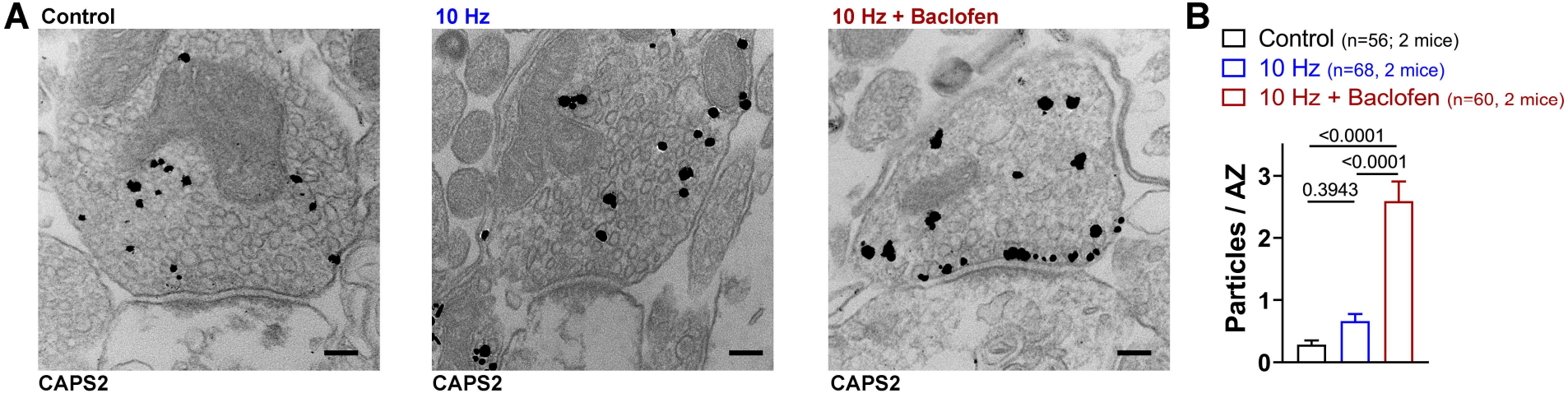
A
Control
10 Hz
10 Hz + Baclofen
CAPS2
CAPS2
CAPS2
B
Control (n=56; 2 mice)
10 Hz (n=68, 2 mice)
10 Hz + Baclofen (n=60, 2 mice)
<0.0001
<0.0001
0.3943
Particles / AZ
0
1
2
3

Figure 8

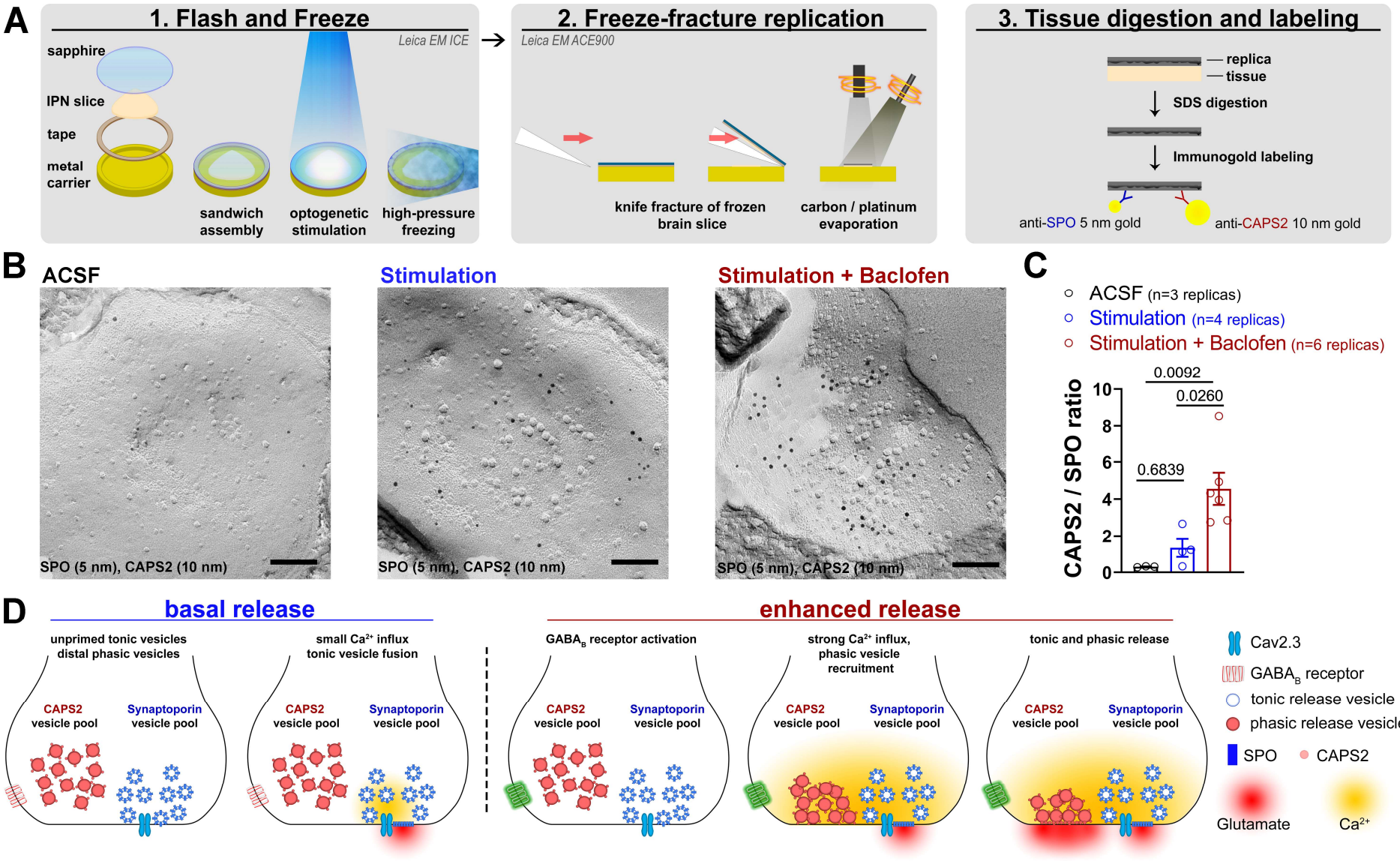
A
1. Flash and Freeze
Leica EM ICE
sapphire
IPN slice
tape
metal carrier
sandwich assembly
optogenetic stimulation
high-pressure freezing
2. Freeze-fracture replication
Leica EM ACE900
knife fracture of frozen brain slice
carbon / platinum evaporation
3. Tissue digestion and labeling
replica
tissue
SDS digestion
Immunogold labeling
anti-SPO 5 nm gold
anti-CAPS2 10 nm gold
B
ACSF
Stimulation
Stimulation + Baclofen
SPO (5 nm), CAPS2 (10 nm)
SPO (5 nm), CAPS2 (10 nm)
SPO (5 nm), CAPS2 (10 nm)
C
ACSF (n=3 replicas)
Stimulation (n=4 replicas)
Stimulation + Baclofen (n=6 replicas)
CAPS2 / SPO ratio
0.0092
0.0260
0.6839
D
basal release
enhanced release
unprimed tonic vesicles
distal phasic vesicles
small Ca2+ influx
tonic vesicle fusion
GABAB receptor activation
strong Ca2+ influx,
phasic vesicle
recruitment
tonic and phasic release
CAPS2
vesicle pool
Synaptoporin
vesicle pool
Cav2.3
GABAB receptor
tonic release vesicle
phasic release vesicle
SPO
CAPS2
Glutamate
Ca2+